A Finite Element Investigation of Possible Mechanisms of Luminal Cell Escape from the Mammary Duct: An Initial Step in Breast Cancer Metastasis

by

Jae Kang

A thesis

presented to the University of Waterloo

in fulfillment of the

thesis requirement for the degree of

Master of Applied Science

in

Civil Engineering

Waterloo, Ontario, Canada, 2017

Author's Declaration

I hereby declare that I am the sole author of this thesis. This is a true copy of the thesis, including any required final revisions, as accepted by my examiners.

I understand that my thesis may be made electronically available to the public.

Abstract

Cancer is an illness that kills some ten million people every year, and as cancer rates increase, a cure for metastatic disease is more necessary than ever. Breast cancer is the most common form of malignancy in the female population, with 1 in 8 women developing invasive ductal carcinoma (IDC) in their lifetime. The majority of cancer deaths are caused by metastasis, a process in which cancer cells spread throughout the body and invade multiple vital organs as a result of increased motility.

Cell biomechanics is a nascent field in oncology, and it investigates cell movement and rearrangement in terms of mechanical forces and deformations. The Differential Interfacial Tension Hypothesis (DITH) provides a way to calculate the net tensions that subcellular components generate along cell boundaries and that give rise to deformation and rearrangement of individual cells and groups of cells. Finite element (FE) software can be used to model these forces and their interactions with each other. To date, this approach has made it possible to study a wide range of morphological phenomena, including wound healing, organ development and metastatic cell migration.

The goal of this study was to use this software to investigate the escape of a single luminal epithelial (LE) cell from a mammary duct – the first stage of breast cancer metastasis. Mechanisms that were considered include: modified interfacial tensions (MIT), protrusions (P) and tension gradients (TG).

The simulations showed that escape of a metastatic LE cell involves two consecutive stages – detachment from the mammary duct and migration through the extracellular matrix. The simulations showed that MIT alone can produce LE cell detachment, while protrusions alone or tension gradients alone can produce migration of cells through the ECM; Mechanisms can act in concert to speed escape and migration, and no single mechanism is able to produce both escape and migration.

The simulations reflect behaviours seen in experiments in organoids and other in vitro systems, adding support for the simulation findings.

Hopefully, the insights provided by this study will help lead to better understanding of the mechanics of cancer cell escape and migration, and to improved strategies for metastasis prevention.

Acknowledgements

I would like to express my utmost gratitude to my supervisor Professor Brodland. I will never forget his patience, kindness and love toward his students, shown through his guidance. Thank you for giving me this invaluable opportunity to apply my engineering knowledge from undergraduate career to cancer research.

I would like to extend many thanks to Jim Veldhuis. Without you, none of the simulations in this study would have been possible.

Mother, Father, Eunice - I cannot possibly express my gratitude for your unconditional support and unparalleled love. Thank you.

Table of Contents

List of Figures

List of Tables

List of Equations

Chapter 1 : Introduction

In order to understand cancer, it is necessary to understand cells, the basic building blocks of life. A cell is the smallest functioning unit of life, and like any organism, it consumes and spends energy to function and reproduce during its lifespan. Some cells thrive on their own, whereas others in a group form a complex multicellular organism. Species of multicellular organisms are made of as few as thousands to as many as quadrillions of cells, and each of them serves its specialized role and coordinates with each other; the unified arrangement and coordination of innumerable cells create extraordinary beings such as humans.

Among the unification, however, some cells behave abnormally as their genes undergo faulty mutations. An abnormal cell exhibits inactivity, underactivity or hyperactivity of either its function, motility, reproduction or the combination of all of them. Some mutated cells are benign and do not affect the overall system or organism to which they belong, whereas others are malignant, which may proliferate in an alarming rate and infiltrate vital organs, disrupting their functions. These malignant cells invade organs by absorbing nutrients, consuming and pushing out their normal-functioning neighbouring cells. The invasion caused by mutated epithelial cells is known as cancer.

In 2012 alone, more than 14 million people were diagnosed with cancer worldwide, and 8 million died from it (Cancer Research UK, 2014). Countless people have died from cancer, and without a cure for it, cancer will continue to be one of the most dreaded diseases of humanity. One of the most common cancer types is breast cancer, which is the most prevalent type in the female population (Cancer Research UK, 2014). The majority of breast cancers originate in mammary ducts (Wasif, Maggard, Ko, & Giuliano, 2010). The invasion of mammary ducts itself is not threatening since their function is not vital for survival (Adriance, Inman, Petersen, & Bissell, 2005). However, the abnormal cells may undergo

metastasis, a process whereby they spread from their original tumour and invade other vital organs including the lungs, liver and brain. Metastasis is difficult to detect at its initial stage, and by the time the patient notices the symptoms, the primary tumour has already metastasized throughout their body, making treatment extremely difficult or impossible. Indeed, fully ninety percent of cancer deaths are caused by metastasis (Mehlen & Puisieux, 2006).

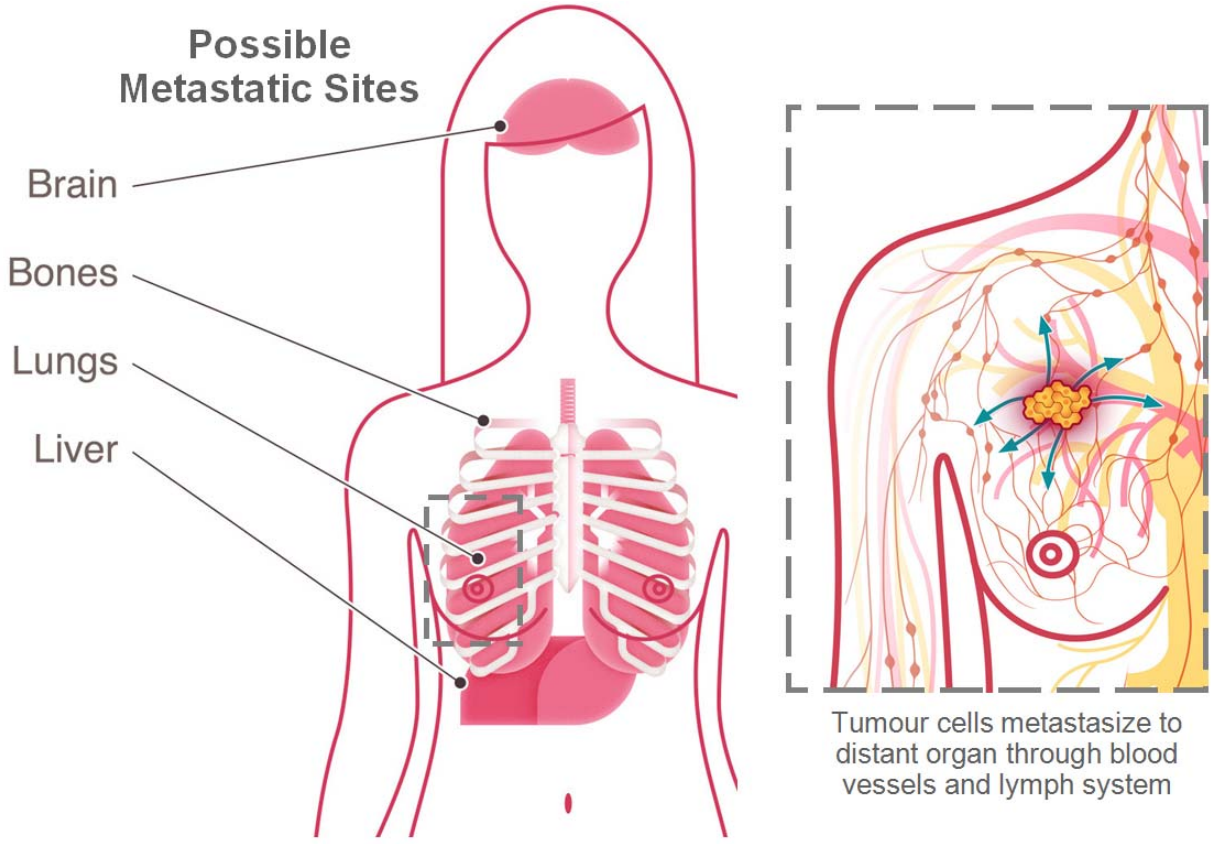

Figure 1.1: Distant Metastasis from Breast to Other Organs
(National Breast Cancer Foundation Inc, 2016)

Metastasis involves changes in cell and tissue morphology, including cell deformation and rearrangement. Morphological changes are not inherently problematic as cells in organisms constantly rearrange themselves, especially during embryogenesis, wound healing and growth (Brodland et al., 2014). Even in mature organisms, although cells seem static, they slowly rearrange themselves as they grow, divide and die (Macias & Hinck, 2012). While it is apparent that a cell deforms due to forces

generated by the cytoskeleton, many of the underlying causes and processes of multiple cell rearrangements still remain unknown, especially in the context of oncology.

Cellular biomechanics, the study of the mechanical behaviours of cells and tissues has gained traction over the last sixty years. In the early years of biomechanics, researchers were only able to analyze the mechanical behaviours of larger components of organisms such as bones, muscles and organs. However, scientists and engineers have developed methods and technologies that can determine the mechanical properties of objects as small and complex as cells (Borghi et al., 2012; Campàs et al., 2014; Guo, Sachs, & Meng, 2014; Hutson et al., 2009; Kasza, Vader, Köster, Wang, & Weitz, 2011; Legant et al., 2010; Maître et al., 2012; Maître, Niwayama, Turlier, Nédélec, & Hiiragi, 2015; Morimatsu, Mekhdjian, Adhikari, & Dunn, 2013; Sugimura, Graner, & Lenne, 2015; Tambe et al., 2013; Thomas, Burnham, Camesano, & Wen, 2013).

Since the 1950s, morphologists hypothesised various mathematical theories regarding the mechanisms of cell deformations and rearrangement (Brodland, 2004). In 2000, Brodland devised the Differential Interfacial Tension Hypothesis (DITH), a theory that describes the interfacial tensions (IT) that govern the deformation and rearrangement of cells (Chen, 2000). Using the DITH, one can identify the cell components that cause certain deformations and arrangements of cells (Krens et al., In preparation), providing insight into their mechanics and to biological experiments. The Brodland lab developed finite element (FE) software that simulates cell tissue morphology based on the DITH. The DITH-based FE software can be used to simulate a variety of real-world cell phenomena including morphogenesis, disease processes, wound healing, tissue engineering and cancer metastasis (Brodland, 2015).

Biologists continue to investigate the causes of the changes to gene regulation associated with cancer (Dachs, Dougherty, Stratford, & Chaplin, 1997; El-Aneed, 2004; J, 2007; Stéhelin, 1995; Ventura & Merajver, 2008). These studies suggest that metastatic cells re-acquire proliferative and motile

properties expressed in embryonic cells. However, while the proliferation rates and rearranging movements of embryonic cells are regulated, those of cancer cells are not (Monk & Holding, 2001). With this in mind, Neumann et al. (In preparation) conducted a genetic experiment on the cells of developing mammary ducts, to understand the behaviour of both embryonic cells and cancer cells (Monk & Holding, 2001). From that experiment, Neumann et al. (In preparation) found three mechanisms of luminal epithelial (LE) cells that drive the elongation of a mammary duct: protrusion, tension gradient and boundary capture. In collaboration with Neumann et al. (In preparation), the Brodland lab simulated the elongation of a mammary duct using the DITH-based FE software and adding capabilities to replicate these three mechanisms of the LE cells.

The goal of current study is to use the DITH-based FE software to simulate and better understand the first stage of metastasis; namely, a single LE cell escaping from a mammary duct.

This study was conducted to answer following questions:

1. In terms of the DITH, what mechanical conditions are necessary for LE cell escape?
2. What are the biological implications of these findings, including:
    a. What cytoskeletal metastatic traits are required for a LE cell to escape from the mammary duct?
    b. Can the mechanisms exhibited by embryonic LE cells during mammary duct development also drive cancer metastasis?

These simulations considered modified interfacial tensions (MIT), as well as the protrusion and tension gradient mechanisms developed by Neumann et al. (In preparation). They were applied to a potentially metastatic LE cell to assess whether or not it would cause it to detach from the mammary duct and migrate through the surrounding tissue. Parametric studies of these mechanisms were used to quantify the escape and migration conditions. The biological implications of the findings were also reflected upon.

It is hoped that the findings of this research will lead to improved understanding of the causes of cancer cell escape and strategies for prevention of cancer metastasis.

Chapter 2 : Literature Review

This chapter outlines current knowledge relevant to the structure of the mammary duct, cancer metastasis and the DITH, and then discusses the DITH-based FE software features that replicate the protrusion, tension gradient mechanisms. A detailed demonstration of the DITH-based FE simulation is included in Section 2.1.3 to aid the reader to better understanding the DITH-based FE approach.

2.1 Computational Biomechanics of Cell Morphology

This section recounts the history of research on cell morphology and introduces the DITH. The DITH-based FE software is then explained, followed by its real-world application and biological significance.

2.1.1 History

One of the first major breakthroughs of cell rearrangement research occurred in 1955, when Holtfreter conducted experiments in which he placed three heterotypic embryonic cells into a solution, and observed them rearranging into the same particular embryo structure repeatedly (Steinberg, 2007). Despite their random placement in the solution, observing the successful rearrangement of the cells over multiple experiments, Holtfreter concluded that cells have inherent properties to sort themselves (Steinberg, 2007).

In the 1960s, Steinberg introduced the Differential Adhesion Hypothesis (DAH), the first widely accepted cell rearranging theory. Steinberg (1975) devised the DAH, presuming that a specific value of adhesion strength exists for each type of cell-to-cell or cell-to-matrix interface. For instance, consider an aggregate formed with two cell types called Cell X and Y, which includes three types of interfaces: X-X (which denotes an interface adjoining one Cell X with another Cell X), Y-Y and X-Y; and each of them consists of its own adhesion strength. If the aggregate is enclosed in a matrix, then there also would be

two more types of interfaces: X-Matrix and Y-Matrix. Figure 2.1 below shows Cell X and Cell Y adjoined with each other surrounded by the matrix, with five types of interfaces.

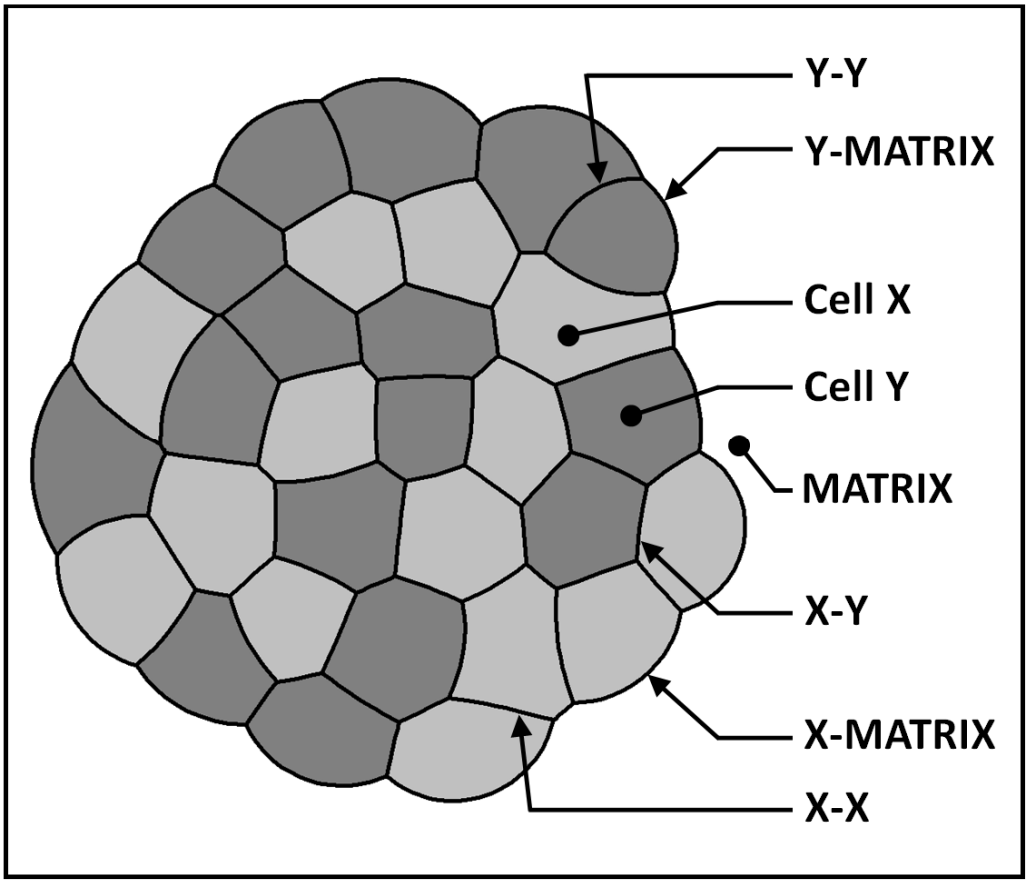

Figure 2.1: Cell X and Y Enclosed in Matrix

The DAH was based on the idea that the rearrangement of cells is driven solely by differences between boundary-specific interfacial adhesion strengths. In the experiment shown in Figure 2.2, darkly-pigmented retina tissue cells are engulfed by translucent neural retina cells (Armstrong, 1989). Initially the cells were mixed in Figure 2.2a, but as time passed the dark cells collected together. In this experiment, dark cells are believed to clump together in the centre because the Dark-Dark adhesion strength is relatively higher than that of the other types of interfaces. Since DAH was introduced, researchers have relied on it to explain various rearranging phenomena of their experiments, and also developed DAH-based computational models (Brodland, 2004).

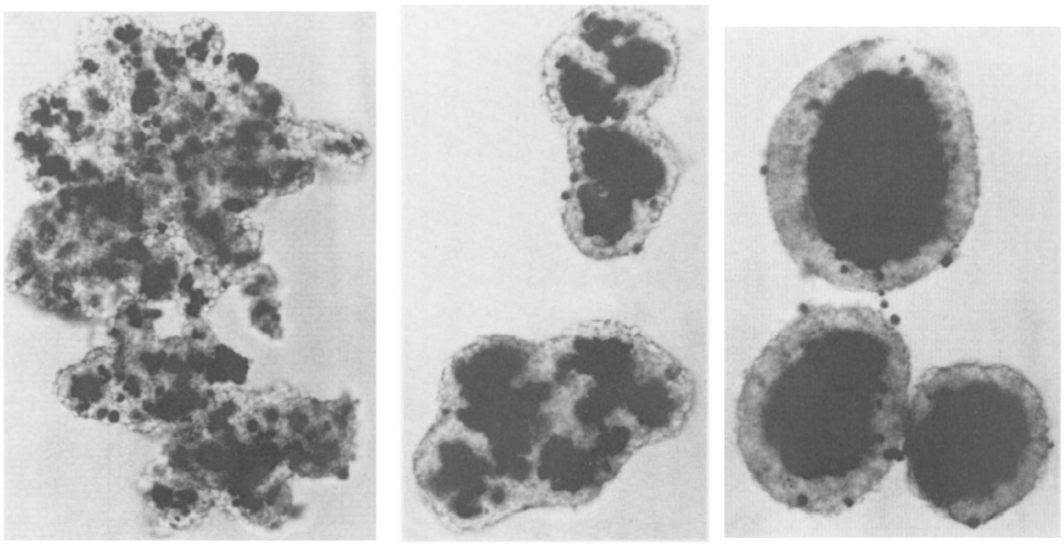

a b c

Figure 2.2: Time-Lapse Microscopic Images of Retina Tissue Cells Engulfing Neural Retina Cells
(Armstrong, 1989)

2.1.2 Differential Interfacial Tension Hypothesis

In 2002, Brodland introduced the Differential Interfacial Tension Hypothesis (DITH), which makes the assertion that cells in a tissue rearrange themselves as a result of differences between their *interfacial tensions* (ITs). According to this theory, in addition to adhesive strength between cells as in the DAH, considers all the cytoskeletal forces (Figure 2.3). Thus, a specific value of tensile force exists for each type of cell-to-cell or cell-to-matrix interface (Brodland, 2004). The intermediate filaments (IFs) and microtubules provide internal structural support of an individual cell, whereas cell adhesion molecules (CAMs), such as desmosomes, cadherin and integrin, provide structural links between one cell and another cell or between a cell and matrix (Brodland, 2004).

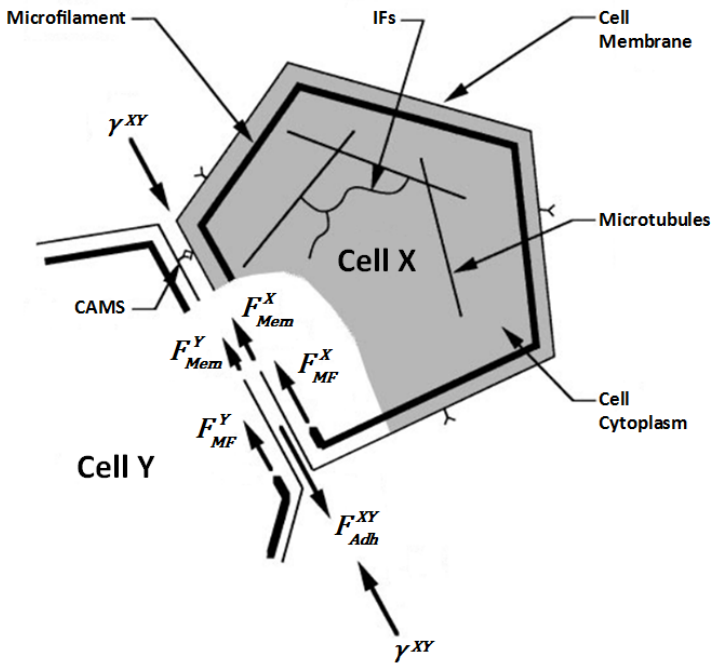

Figure 2.3: Force Generating Structral Components of Cell-to-Cell Interface
(Brodland, Viens, & Veldhuis, 2007)

In 2004, the Brodland group devised an equation that determines the net IT of an interface adjoining two cells. In this theory, the membrane together with cortical microfilaments and other protein systems near the membrane of each cell generate tensile forces at the interface, while adhesion reduces it (Figure 2.3). For an interface between two cells denoted Cell *X* and *Y* the force is:

$$\gamma^{XY} = F^X_{Mem} + F^Y_{Mem} + F^X_{MF} + F^Y_{MF} - F^{XY}_{Adh} + F^{XY}_{Other}\,, \tag{1}$$

where the variables are (Brodland, 2004):

- γ^{XY}: net IT of the interface adjoining Cell *X* and *Y*
- F^X_{Mem}: contractile (tensile) force at the interface contributed by Cell *X* membrane
- F^Y_{Mem}: contractile force at the interface contributed by Cell *Y* membrane
- F^X_{MF}: contractile force at the interface contributed by Cell *X* microfilaments
- F^Y_{MF}: contractile force at the interface contributed by Cell Y microfilaments
- F^{XY}_{Adh}: equivalent force contributed by the elongation of cell interface due to the adhesion of Cell *X* and *Y*
- F^{XY}_{Other}: Other contractile force due to any other miscellaneous factors

F_{Adh}^{XY} in Equation 1 is negative because as two cells adhere, the adjoined interface tends to elongate, and that reduces the IT. F_{Other}^{XY} accounts for the forces by any other subcellular components that contribute to IT including intermediate filaments and microtubules, as well as any other force exerting components still to be identified (Brodland, 2004).

Equation 2 represents the net IT of an interface along an interface where a Cell *X* is in contact with matrix Figure 2.4 (Brodland, 2004):

$$\gamma^{XM} = F_{Mem}^{X} + F_{MF}^{X} - F_{Adh}^{XM} + F_{Other}^{XM} \tag{2}$$

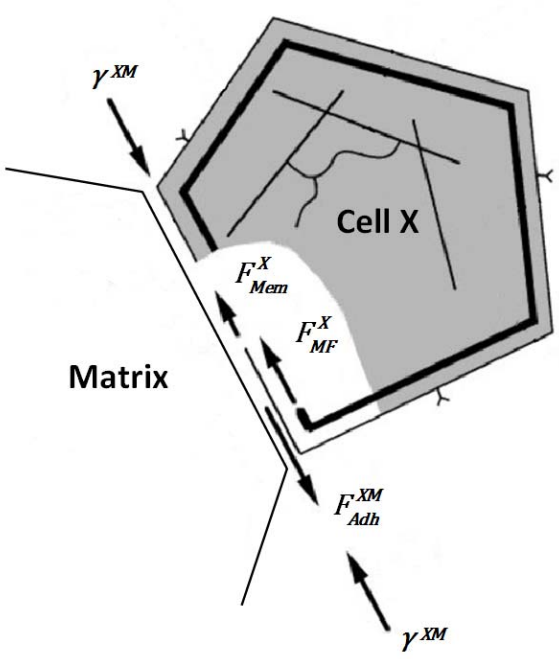

Figure 2.4: Force Generating Structral Components of Cell-to-Matrix Interface
(Brodland et al., 2007)

Similar to F_{Adh}^{XY}, F_{Adh}^{XM} represents the equivalent force of elongation of a cell interface due to the adhesion between Cell *X* and the matrix, and F_{Other}^{XM} includes other contractile force due to miscellaneous cell matrix component that contributes to cell-matrix IT.

According to the DITH, a specific IT exists for each cell-to-cell or cell-to-matrix interface: the IT varies depending on the types of the cells or matrix associated with each interface. These forces are resisted by the viscosity of the cytoplasm and other internal components of the cell, and they are represented by a viscosity μ. When IT imbalance arise, the edges of cells may shorten or elongate, causing cell deformation and possibly rearrangement (Brodland, 2004). These motions can be modelled using finite element software, as described next.

2.1.3 The Finite Element Model

Conventional Triangle Element Method

The finite element method is well known in engineering and physics (Lewis, Nithiarasu, & Seetharamu, 2004; Potts & Zdravkovic, 2001; Zienkiewicz, Taylor, & Fox, 2014; Zienkiewicz, Taylor, & Nithiarasu, 2014). However, certain modifications are required if it is to be used to analyze cell mechanics. Chen and Brodland (2000) developed the first two-dimensional FE software for cell mechanics based on the DITH. In the software, the volume (area) of each modelled cell is divided into viscous triangle elements (Figure 2.5), as in a standard FE model. Each junction, at which more than two edges meet, is set as a node, and the interface between the junctions is treated as an element edge. Each edge is assigned a net IT, such as γ^{LD} (Brodland & Chen, 2000b).

An additional node is added to the centroid of the cell, and internal edges are traced from the center node to each edge nodes, causing each cell to be divided into triangle elements. Doing so allows the use of conventional triangle shape functions for area modeling. In order to maintain the area of each cell, the sum of the triangle areas each cell is constrained using a Lagrange side condition (Brodland & Chen, 2000b). Since the normal motions of cells are not fast enough to produce inertial forces, cells are considered to be in a quasi-static state. For this reason, no inertia forces need be considered.

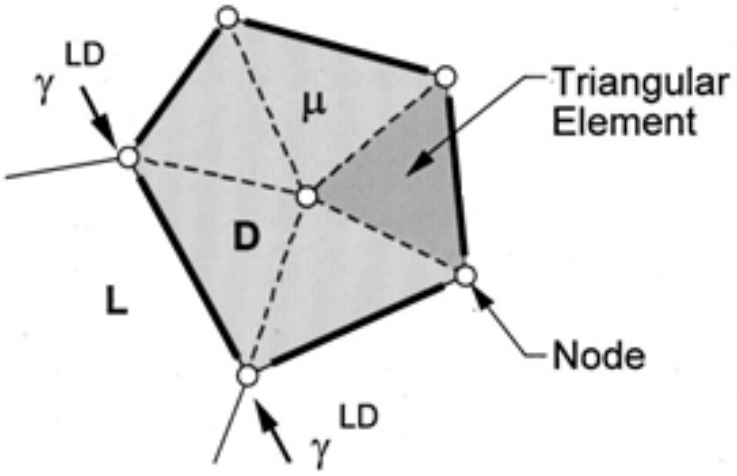

Figure 2.5: Cell Discretized into Triangular Elements
(Brodland & Chen, 2000)

This FE model has been used to successfully investigate a wide range of cellular phenomena, such as cell sorting and engulfment. However, this software has a limitation; the triangular elements become stiffer as their edges become shorter (Viens & Brodland, 2007). As a result, cells containing narrow triangular elements displayed a so called 'stiffening artifact' (Viens & Brodland, 2007).

Dashpot Approach

To overcome this difficulty, Brodland, Viens and Veldhuis (2007) developed a dashpot approach. In this method, two sets of viscous dashpots, one parallel to the long of the cell and the other parallel to the perpendicular short axis (Figure 2.6), are attached to every node to capture the stress-strain constitutive equation of the cytoplasm (Viens & Brodland, 2007). All of the dashpots in each direction are interconnected to each other, so that when one node displaces, the dashpots distribute forces of the equivalent magnitude to the rest of the nodes in a cell (Viens & Brodland, 2007). For instance, when a force *f* is applied to a node, the rest of the nodes in the cell are subjected to a magnitude of force equivalent to *f* divided by the number of the nodes in the cell minus one, excluding the node the force is applied.

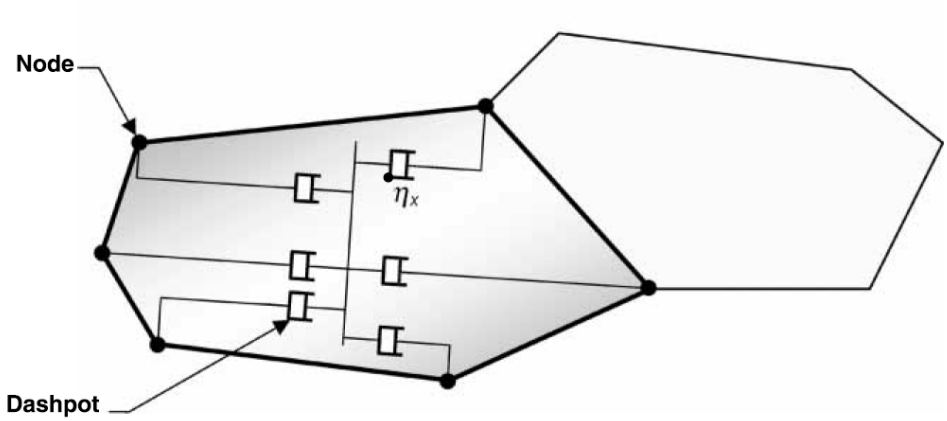

Figure 2.6: Meshed Cell with Dashpots on Nodes
(Brodland et al., 2007)

Using standard FE procedures, the dashpot and IT forces can be used to construct a single matrix equation:

$$\frac{1}{\Delta t}\mathbf{C}\cdot\mathbf{u}=\mathbf{f} \tag{3}$$

where $\mathbf{C}$ is the equivalent viscosity matrix and $\mathbf{f}$ is the nodal force resultants from the ITs. This equation is solved for the node displacements $\mathbf{u}$ due to the ITs exerted during each time step Δt of the FE analysis. Boundary conditions and cellular volume constraints are imposed through Lagrangian side conditions.

Polyline Enhancement

Recent studies have shown that cell rearrangement can be affected by an artifact associated with the use of straight cell interfaces (Perrone, Veldhuis, & Brodland, 2016). This artifact can be overcome by replacing the standard straight interfaces with polyline interfaces, as shown in Figure 2.7. Details of the associated mathematics and its implementation are reported in detail elsewhere and are not repeated here. This approach is used in all of the simulations reported here.

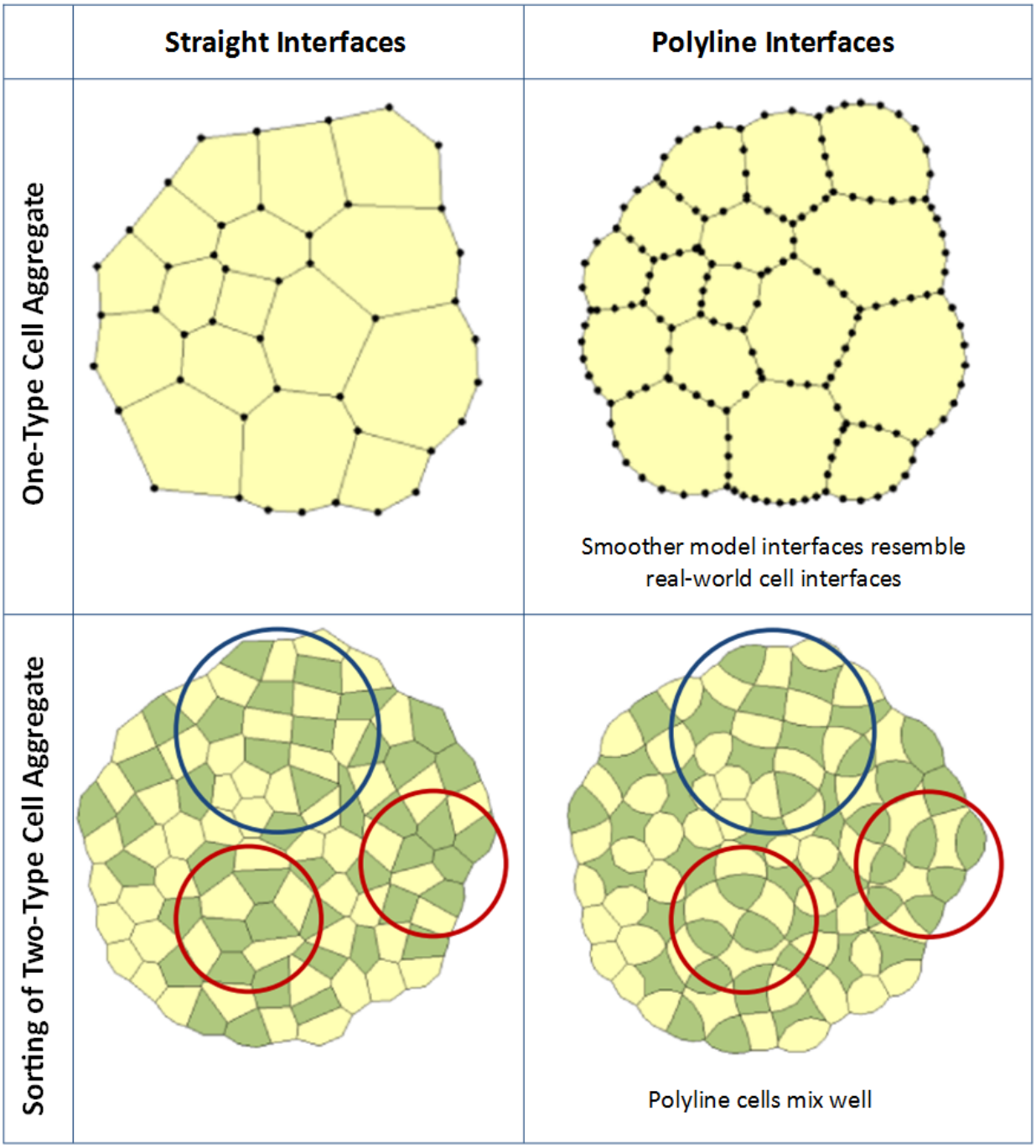

Figure 2.7: Straight Interfaces VS Polyline Interfaces
(Perrone et al., 2016)

Example

To illustrate how ITs can drive specific patterns of cell motion, simple four-cell model simulations are presented (Table 2.1, Figure 2.8). All four models begin from the same initial geometry consisting of two so-called red (R) and two green (G) cells surrounded by matrix (white space). The system has four types of interfaces: Red-Green, Red-Red, Red-Matrix, and Green–Matrix. According to the DITH, each type of interface has its own corresponding IT. The Red-Green, Red-Red, Green-Green, Red-Matrix, and Green–Matrix ITs are denoted γ^{RG}, γ^{RR}, γ^{GG}, γ^{RM} and γ^{GM}, respectively.

Two boundary conditions were defined: one node was fixed in x- and y- directions, while another was fixed in x-direction so that the tissue does not displace or rotate arbitrarily. In addition, the area of each cell was set to remain constant throughout the duration of the simulations. The red and green cells are assigned the same viscosity, whereas the matrix is not viscous. The only effect of the viscosity is that it regulates the rate at which cell motions occur.

Four simulations were conducted with varying combinations of ITs (Table 2.1), and each was run until steady-state was reached (Figure 2.8).

Table 2.1: Interfacial Tensions of Four-cell Model Simulation Cases

Case	γ^{RR}	γ^{RG}	γ^{GG}	γ^{RM}	γ^{GM}
b	1	1	1	1	1
c	1.5	1	1	1	1
d	1	1.5	1	1	1
e	1	1	1	1.5	1.5

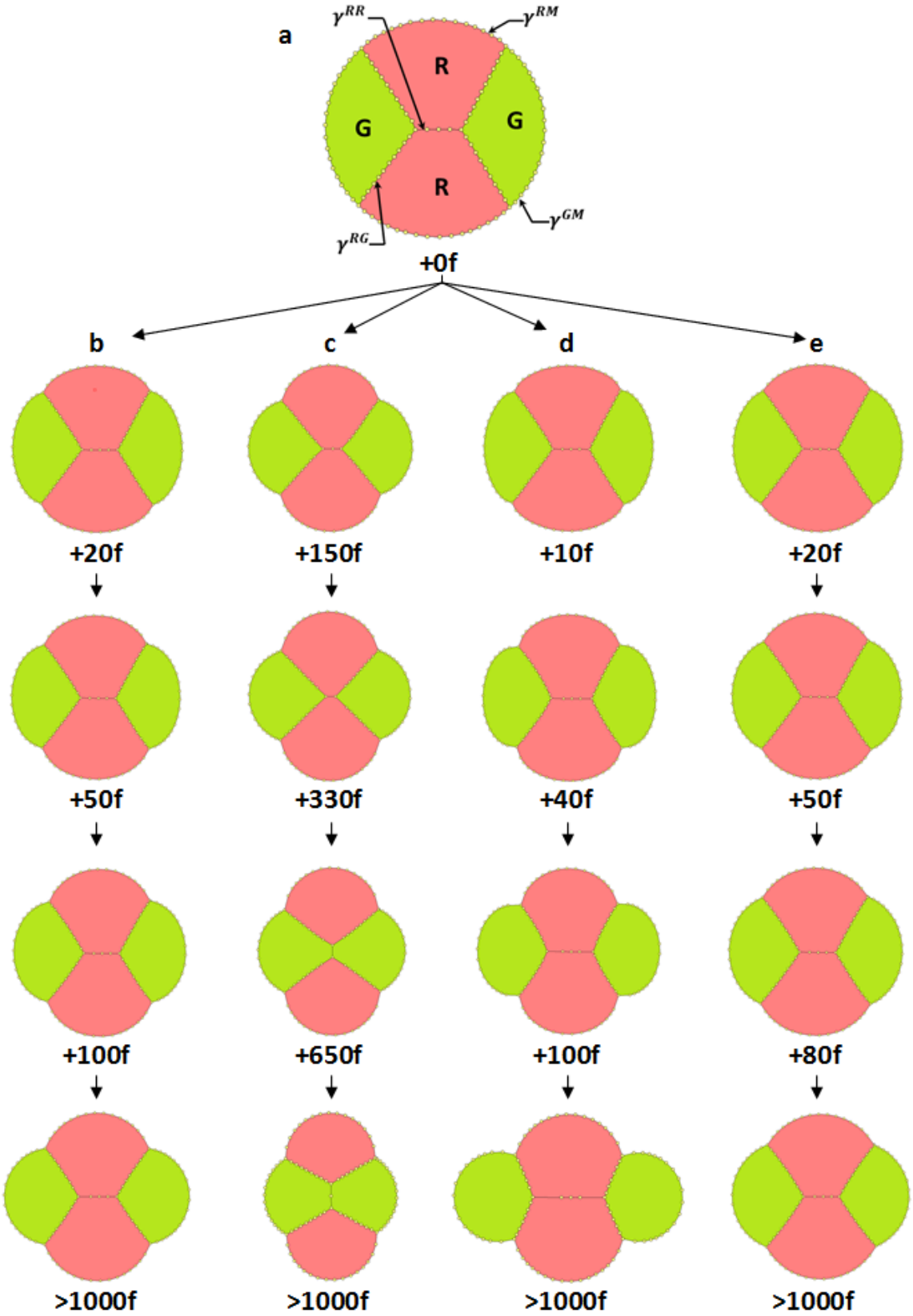

Figure 2.8: Initial to Steady-state Geometry of Four-cell Model Configurations

For the simulation in Case b, every edge exerts the same IT, whereas in Case c the Red-Red interface edges exert 1.5 times stronger IT than other interface edges. Likewise, Case d and e were simulated with one type of interface 1.5 times greater than the rest.

In each time step, every node experiences a corresponding resultant force from the ITs exerted by the joining edges in the current geometry. Nodes continue to displace in every time step and eventually reach steady-state when all of the resultants eventually converge to zero. There are two types of nodes in the FE model: edge nodes that involve two cells and surrounding matrix, and triple junctions (TJ), where three edges from a trio of close-packed mutually contacting cells converge.

If all of the edges at a particular TJ carry the same IT, one would expect the angles formed to be equal, and both are the case for the TJs shown in the steady-state of Case b.

Figure 2.9 includes several time-lapse images from the Case c simulation. The Red-Red edge shortens from the beginning to Step +498f, and then disappears at +499f. The Red-Red interface shortens since its end TJs (A and B) displace toward each other. The close-up of TJ B at +50f shows that it is pulled by one Red-Red, and two Red-Green edges. *RG1* and *RG 2* refer to the upper and lower Red-Green interfaces.

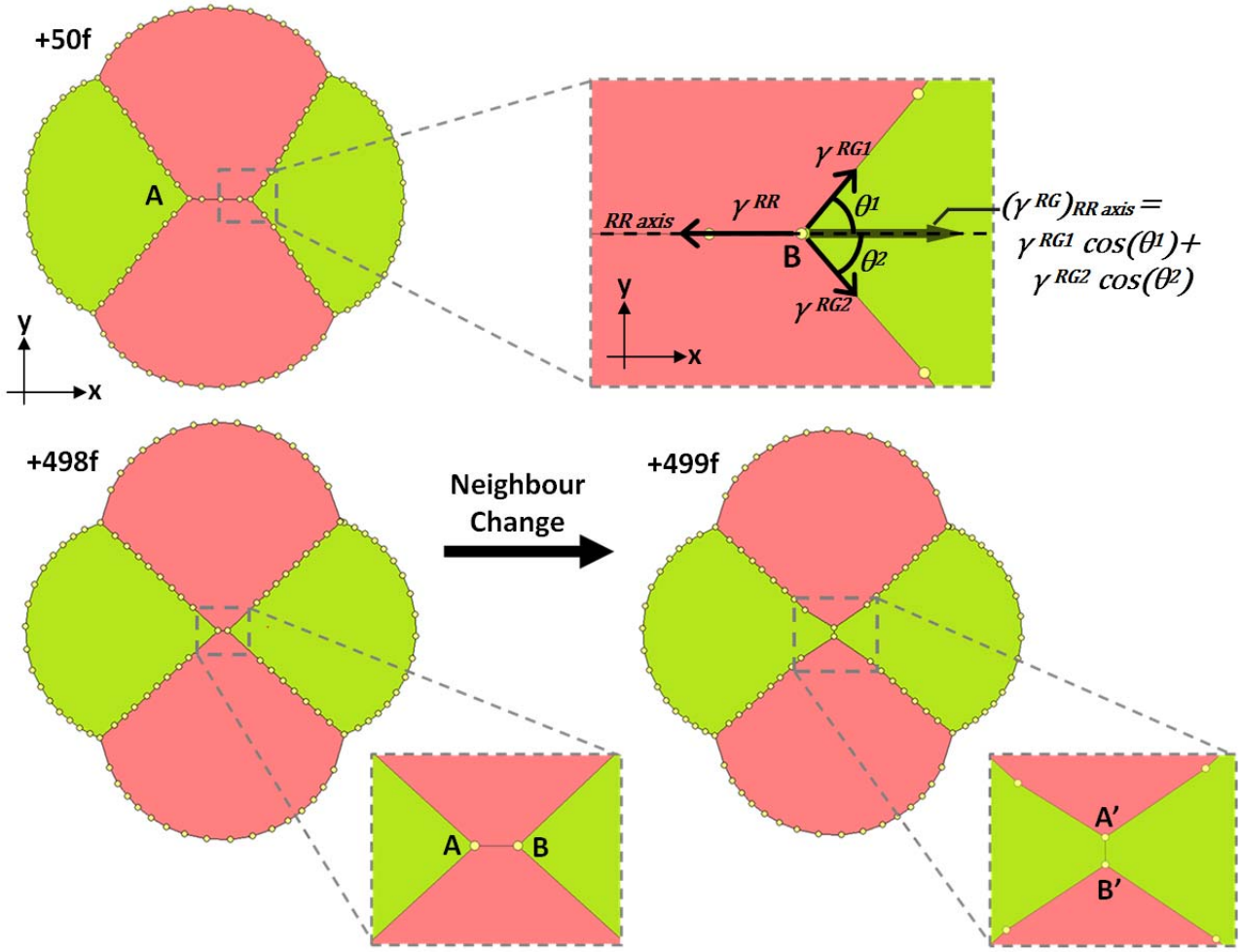

Figure 2.9: Time-lapse Images of Case d Simulation

The FE software computes the ITs and their resultants and the incremental nodal displacements, all with respect to the global x and y axes, one time step after the next. However, this demonstration also shows a special case where the TJ displacement occurs along an axis parallel to one of the incoming ITs. Resultants are frequently analyzed as such because the TJ displacement along a certain interface is often the matter of interest. Figure 2.9 shows the IT balance at TJ B in RR axis. TJ B displaces toward the direction of γ^{RR} since γ^{RR} is greater than the sum of the γ^{RG1} and γ^{RG2} components in RR axis.

This can be expressed in following equation:

$$\gamma^{RR} > (\gamma^{RG1} + \gamma^{RG2})_{Red-Red\ axis}$$

ITs in brackets are the ITs' force components that are parallel to the subscripted axis. The TJs do not move perpendicular to RR axis in this case since the Red-Green edges are symmetric about RR axis. Note that TJ A geometry is symmetrical as TJ B about y axis and hence it also moves in the direction of γ^{RR}.

When significant differences between ITs cause nodes to have high resultant forces, the resulting displacements can cause the node spacing along polyline edges to become quite non-uniform. Large distances between adjacent nodes decrease the smoothness of interface. On the other hand, when the nodes approach unnecessarily close to each other, the simulation becomes computationally inefficient and they are also under the risk of passing each other in the subsequent time step. To prevent adjacent nodes from displacing too far or close from each other, the user of the software can input a desired range of distances to be maintained between adjacent nodes. When the distance between two adjacent nodes is outside the specified range, the software either adds an extra edge node between two far nodes, or removes one of two close edge nodes. These features are referred to as *edge node addition* (ENA) and *edge node removal* (ENR).

In Case c, the shortening Red-Red interface undergoes ENR until only two TJ are left at +498f. As TJ A and B approach toward each other and the distance between them become less than the specified minimum distance of nodes. The software, instead of ENR, removes the existing Red-Red interface and creates the new perpendicular Green-Green interface that borders the green cells (Figure 2.9). This feature known as *neighbour change* removes two approaching TJs and creates a new pair of TJs to establish a new a cell-to-cell contact. In Figure 2.9 (+498f - +499f), the neighbour change feature removes TJ A and B then creates A' and B'. Afterward, the Green-Green interface elongates until the model reaches steady-state.

Neighbour change was added to the FE software to recapitulate the real-world cellular rearrangement where two approaching cells continue to adjoin after establishing their initial contact. Neighbour change does not allow more than three incoming edges for any node.

In Case d, the stronger Red-Green edges shortens, and Red-Matrix and Green-Matrix edges angularly narrow until the TJs reach steady-state.

The simulations show that interfaces with stronger ITs typically shorten, whereas those with weaker ITs lengthen either of which tends to bring about displacements of triple junctions and resulting angular changes. Indeed, simulations can be as associated with a geometrically similar 'tug-of-war' scenarios between the ITs at its nodes.

2.1.4 Biological Significance of the Finite Element Simulations

Although models cannot replace laboratory experiments and prove mechanisms, they allow interpretation of biological experiments from the mechanical standpoint. Brodland's lab has simulated various real-world phenomena, including tissue engineering, wound healing, organ development and cancer cell invasion (Brodland, 2006; Brodland, 2002; Brodland & Veldhuis, 2012; Chen & Brodland, 2008; Neumann et al., In preparation; Vedula et al., 2014). The following are some of the most prominent simulations from Brodland's Lab:

Cell Engulfment

Brodland (2002) simulated the engulfment of cells, which resembles Armstrong's experiment in Figure 2.2, using the DITH-based FE software. Figure 2.10 shows that the dark- and light-coloured cells are mixed together in the initial configuration, and the light cells engulf dark cells at steady-state. Since ITs are mainly generated by the contractions of cell membranes and microfilaments (Equation 1 & 2), a high IT can represent an interface consisting of high membrane and microfilament contractile forces and low adhesive strength between adjoined cells (Brodland, 2004). Equation 1 suggests that weak Dark-Dark IT

consists of weak membrane and microfilament contractions or strong interface adhesions of the dark cells.

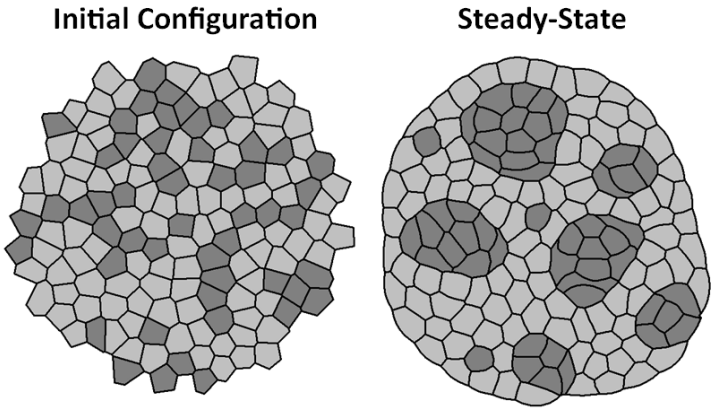

Figure 2.10: FE Simulation of Light-coloured Cells Engulfing Dark-coloured Cells

Neurulation

Chen and Brodland (2009) also created three dimensional DITH-based FE software to simulate neurulation, which is folding phenomenon of a neural plate in a vertebrate embryo that ultimately creates the brain and spinal cord. The three dimensional model was made using extruded triangular elements. Chen and Brodland observed that in order for the plate to fold as shown in the real images in Figure 2.11, the cells need lamellipodia to generate graded lateral tensile forces over neural plate (Chen & Brodland, 2008).

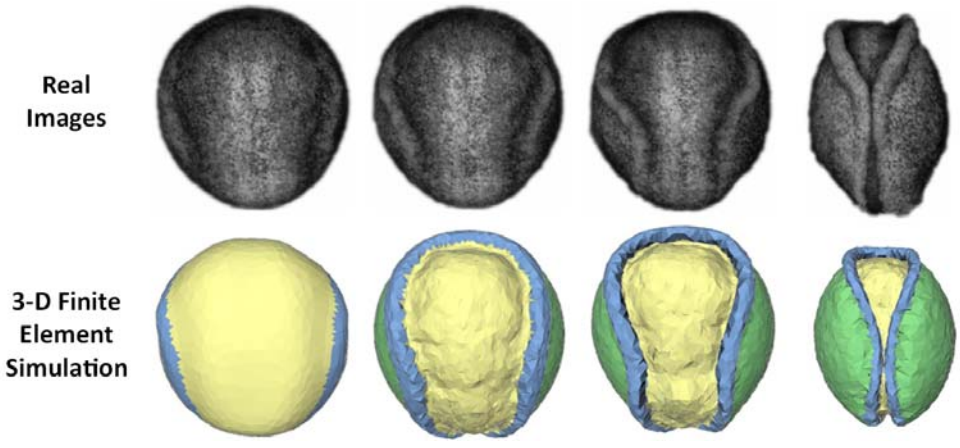

Figure 2.11: Neurulation of an Amphibian Embryo: Real Images vs FE Simulation
(Brodland, Chen, Lee & Marsden, 2010)

These simulations show that the FE software can simulate real-world morphological phenomena with right combinations of initial configurations and ITs. Unfortunately, experiments that measure cells' specific interfacial tensions are not yet available (Brodland, 2002). However, the computational experiments allow one to trace the cause of cell behaviours from different perspective and much likely find new insights. Although biology is the key that explains the root cause of cell behaviours, biomechanics is also essential as it demonstrates how forces generate movements at the molecular, cytoskeletal and cellular levels. As such, this study simulates breast cancer cell metastasis to provide new insights from the mechanical standpoint.

2.2 Mammary Duct

This section provides an outline of the anatomy of the breast and especially the cellular structure of the mammary gland, in which the duct is located. Then it discusses the causes and processes of mammary duct development and breast cancer metastasis.

2.2.1 Anatomy & Physiology

Female Breast

A female breast consists of a mammary gland, an organ that produces and secretes milk, along with the blood and lymph vessels that nurture the gland cells (Figure 2.12). The mammary gland, blood vessels and lymphatic system are enclosed by a layer of extracellular matrix (ECM). ECM is connective tissue made of assembled proteins such as collagen together with protein secreting cells such as fibroblasts. The rest of the breast is filled with body fat (Standring, 2008). The ECM and fatty tissue create and support the shape of the breast, and also protect the mammary gland and its vascular and lymphatic systems.

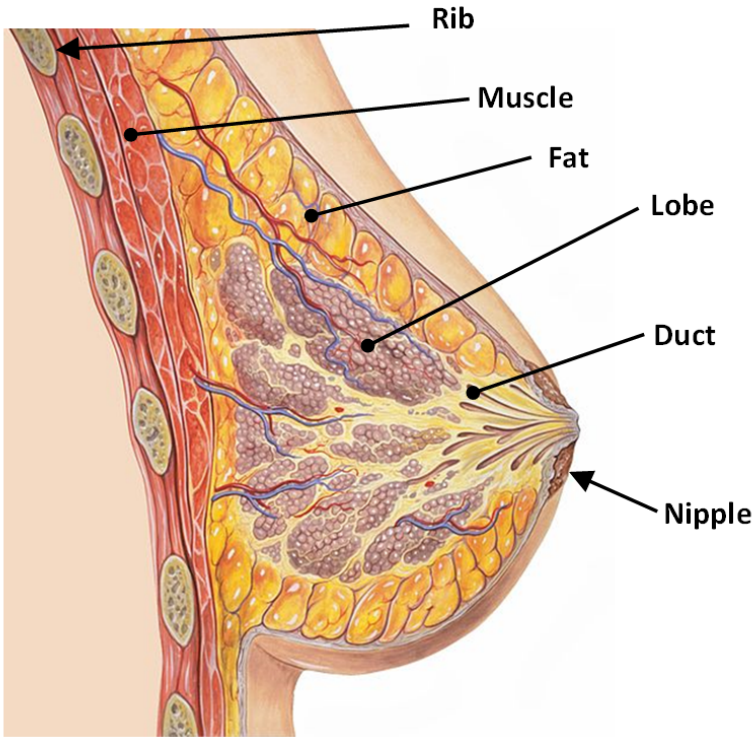

Figure 2.12: Anatomy of Female Breast
(Meyerson, 2016)

Mammary Gland

A mammary gland consists of bundles of mammary lobes, ducts and a nipple (Figure 2.12). The lobes secrete milk during a lactation period, and mammary ducts deliver the milk to the nipple.

A female mammary gland is developed during the embryotic stage, and its structure alters significantly during puberty, pregnancy, lactation and involution (Macias & Hinck, 2012). The mammary gland is developed at the end of puberty and remains in homeostasis until pregnancy. A homeostatic mammary gland does not exhibit any morphological rearrangement, with the exception of mitosis and apoptosis. During pregnancy, the mammary gland develops further with the creation of more ducts and lobules to prepare for lactation. The mammary gland returns to its pre-pregnant state after the lactation period (Macias & Hinck, 2012).

Mammary Duct & Lobes

Mammary ducts and lobes are made of two layers: inner luminal epithelial (LE) and outer myoepithelial (ME) cells (Figure 2.13). The lobes and ducts are enclosed by a layer of basement membrane, and further surrounded by ECM (Adriance, Inman, Petersen, & Bissell, 2005). The duct refers to the pipe-like portion of the mammary gland, and the lobe refers to the end of the gland with acinar cellular architecture (Figure 2.13) (Adriance, Inman, Petersen, & Bissell, 2005). Inside the mammary duct, the LE cells are arranged in a single cuboidal layer and are tightly adhered to the thinly spread out ME layer (Figure 2.13). During the lactation period, the LE cells in lobes secrete milk while the ME cells in lobes and ducts contract and expand to deliver the stored milk from lobes to the nipple (Adriance, Inman, Petersen, & Bissell, 2005).

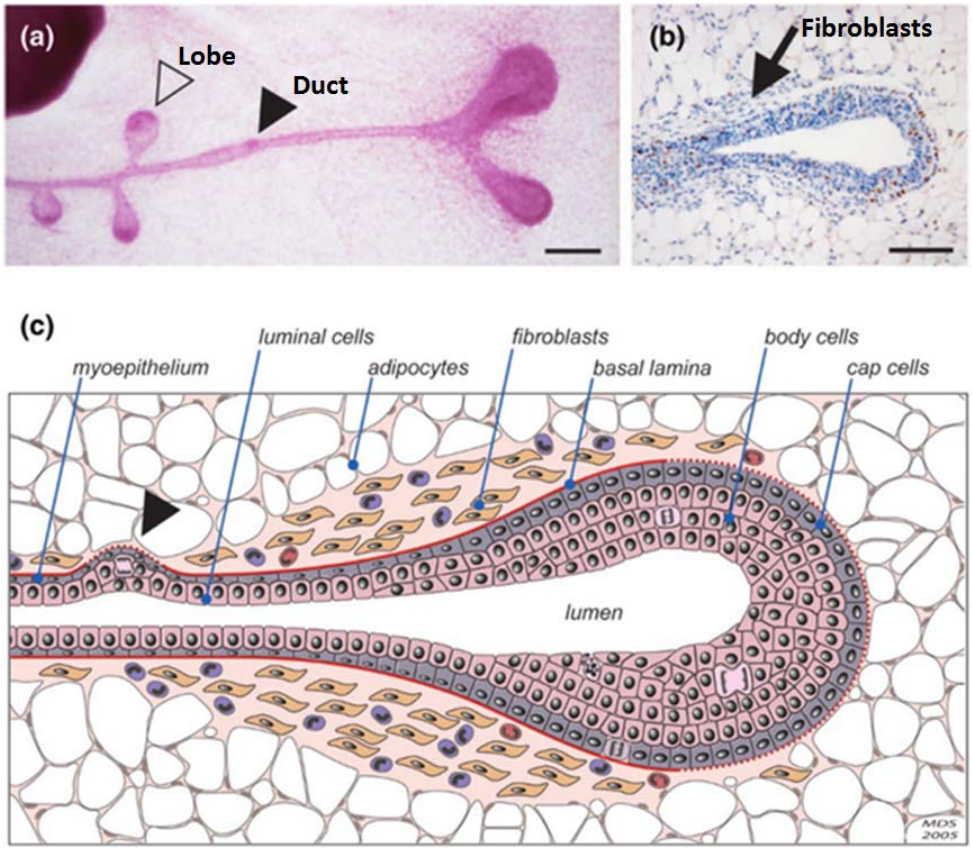

Figure 2.13: Cellular-level Anatomy of Mammary Duct and Lobe: Profile
(Sternlicht, 2006)

Each LE and ME cell in a mammary duct contains a keratin-based cytoskeleton, which serve as the major structural support for homeostatic cells (Adriance, Inman, Petersen, & Bissell, 2005). Additionally, ME cells also contain actin filaments that contract during lactation. In terms of cell-to-cell interaction, ME and LE cells adhere to each other through desmosomes and adhesion molecules such as E-cadherin, as shown in Figure 2.14. The ME cells are joined to each other through cadherins and gap junctions, while adhered to basement membrane through hemi-desmosomes (Adriance, Inman, Petersen, & Bissell, 2005). The cytoskeletal structures and adhesion interactions of the duct cells and ECM are presented in Figure 2.14.

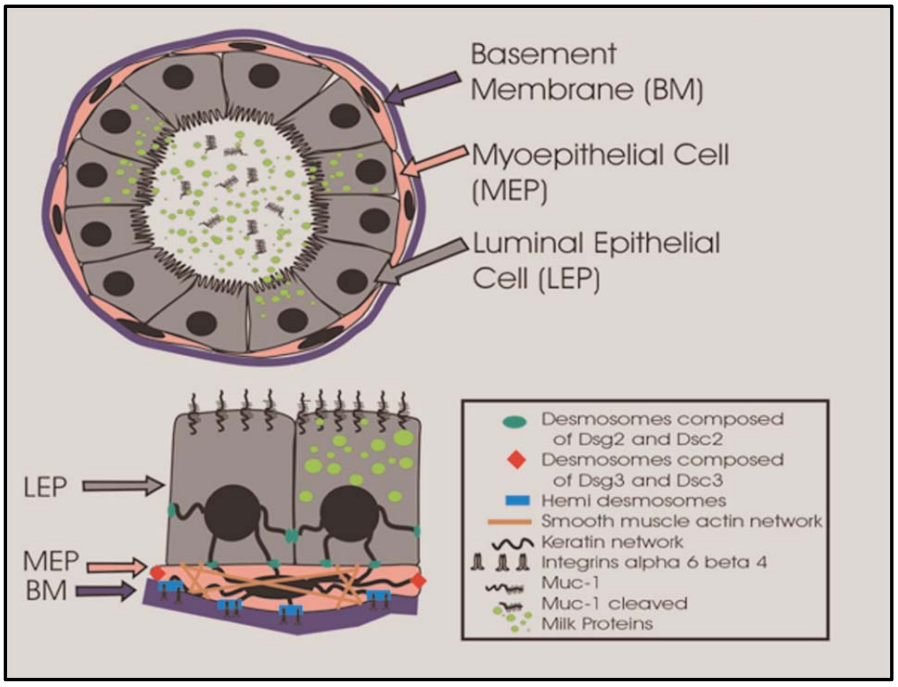

Figure 2.14: Cellular-level Anatomy of Mammary Duct: Cross-section
(Adriance et al., 2005)

2.2.2 Mammary Duct Development through Intercalation

At the beginning of mammary duct development, LE and ME cells originate from an ectoderm layer that eventually gives rise to all of the epithelial cells of a mammal (Macias & Hinck, 2012). Development of the mammary duct occurs in two stages: initial development during the embryonic stage before birth,

and maturing stage through puberty (Macias & Hinck, 2012). During the embryonic stage, the LE and ME cells proliferate rapidly, creating a placode in the mammary stroma as shown in Figure 2.15 (Macias & Hinck, 2012). The proliferating cells arrange themselves into strands that elongate and branch off repeatedly. The cell proliferation ceases after multiple series of elongation and branching, and the LE cells inside rearrange themselves until the bilayer architecture is formed (Huebner & Ewald, 2014). At the end of the embryonic stage, small and simple ducts are formed and they remain dormant until puberty (Huebner & Ewald, 2014).

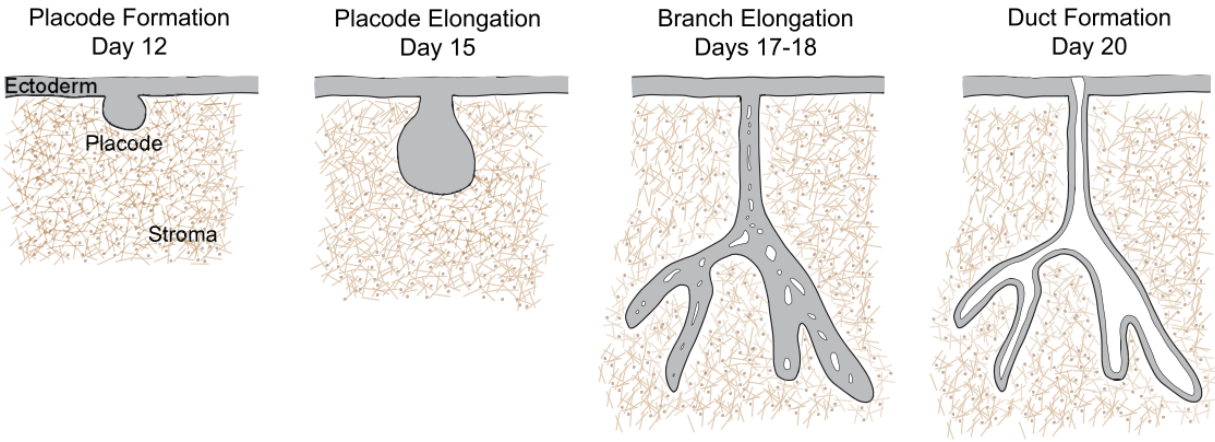

Figure 2.15: Embryonic Mammary Development of Mouse
(Huebner & Ewald, 2014)

As puberty begins, the ducts undergo further elongation and branching morphogenesis, forming much longer ducts with secondary branches (Figure 2.16) (Huebner & Ewald, 2014). The LE cells around the ends of the dormant ducts proliferate and form stratified layers, as shown in Figure 2.13. The LE cells in the lobe continue to proliferate, supplying the cells that form bilayers and elongate the duct to the extent of several centimeters in length in female humans (Huebner & Ewald, 2014). When the growth signals halt at the end of puberty, the proliferation of LE cells ceases, leaving the lobes with several layers of LE cells (Huebner & Ewald, 2014).

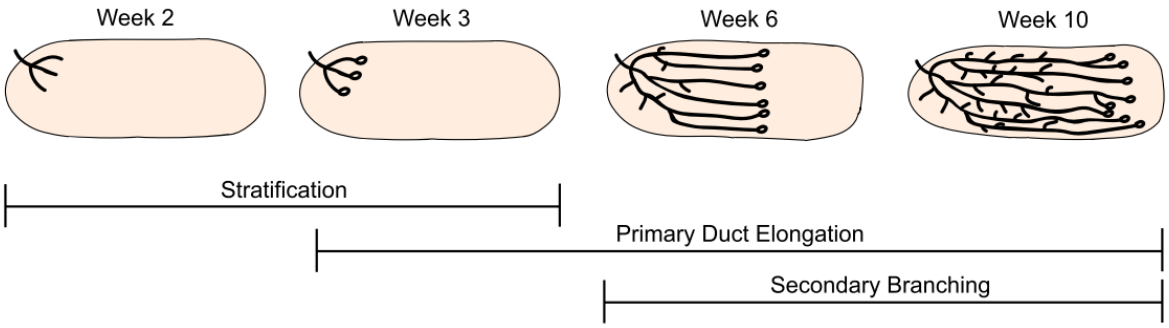

Figure 2.16: Postnatal Mammary Development of Mouse
(Huebner & Ewald, 2014)

Without the technology to observe the actual the development of mammary duct in-vivo, many embryologists could only hypothesize how the LE and ME cells rearrange themselves during the development (Huebner & Ewald, 2014). The most recent hypothesis that explains the morphology of duct development is the radial intercalation of LE cells (Huebner & Ewald, 2014). Intercalation is the action of a cell protruding itself between two adjacent cells. Neumann et al. (In preparation) verified that the LE cells in a lobe intercalate themselves to the most outer LE cell layers and adjoin with the ME layer. Figure 2.17 shows a luminal cell radially intercalating. When all the LE cells in the stratified layers have intercalated, because they are all bordering the ME layer, the duct has indeed formed into the bilayer architecture (Huebner & Ewald, 2014). The intercalation of stratified LE cells in the lobe to a single layer in the duct result in expansion of the duct surface, and hence the duct elongates.

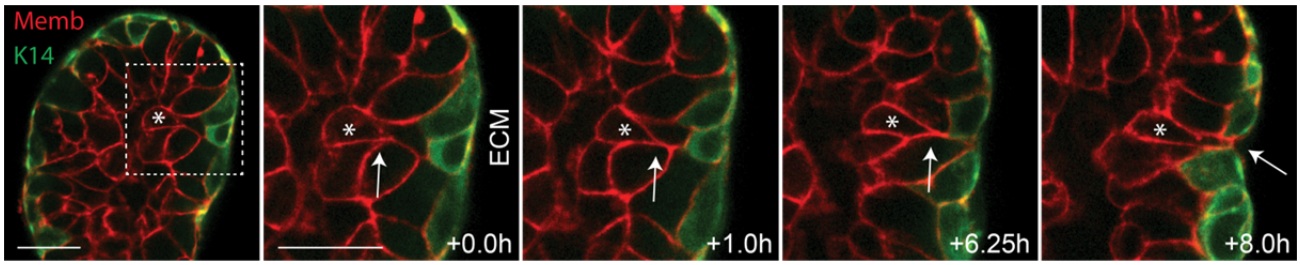

Figure 2.17: Time-lapse Microscopic Images of Luminal Epithelial Cell Intercalation
(Neumann et al., In preparation)

2.2.3 Breast Cancer & Metastasis

Ductal carcinoma is a type of cancer that originates from the mutated LE cells in a mammary duct, and they are the cause of 90% of breast cancers (Wasif et al., 2010). Ductal carcinoma can be further classified into two types: ductal carcinoma in-situ (DCIS) and invasive ductal carcinoma (IDC) (American Caner Society, 2016).

Ductal carcinoma is classified as DCIS when LE cells abnormally proliferate and form a tumour inside a duct. Although these LE cells proliferate and create a large tumour, they stay inside the ME layer, as shown in Figure 2.18 (Bane, 2013). IDC is the lethal type in which the LE cells metastasize. Metastasis refers to the spread of cancer cells to other organs and it is the reason of most cancer deaths (Chambers, Groom, & MacDonald, 2003). These IDC cells must undergo the following steps to successfully metastasize: escape from the mammary duct, entering and exiting a blood/lymph vessel, and invasion of a secondary site. A version of the DITH-based FE software successfully simulated the various steps from escape to invasion of a vessel, and those simulations showed that the properties of the motile cell must change multiple times for this sequence of events to play out (Brodland & Veldhuis, 2012). In IDC, either a single or collective LE cells undergo mutations that cause them to detach from the mammary duct (Shamir et al., 2014) (Figure 2.18).

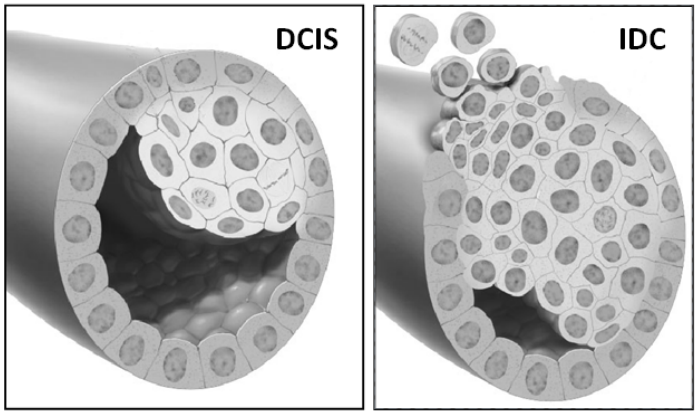

Figure 2.18: Cross-section of Duct: DCIS and IDC
(National Cancer Institute, 2005)

Statistics show that patients rarely die from DCIS because of the fact that cancerous cells do not metastasize from the primary tumor (Roses, et al., 2011). However, in the healthcare industry, DCIS is considered a threat because studies support that there is an increased probability of DCIS progressing into IDC, instead IDC occurring in a normal duct. One of the suggested mechanisms is that uncontrolled proliferation of cancerous cells may induce mechanical stress and produce cues that promote metastasis (Bane, 2013). For instance, Kumar and Weaver (2009) found that increased mechanical stress of cells and ECM due to tumor growth weakens cell-cell and strengthens cell-ECM adhesion, which is considered favorable for the migration of metastatic cells. Adriance et al. (2005) also suggested that the loss of ME function is what leads to metastasis. However, a survey noted that the occurrence of metastasis developed from DCIS is rare (Roses et al., 2011).

In IDC, a mutated LE cell undergoes the alteration of its internal cytoskeletal composition and structure, as well as its interactions with neighbouring cells and ECM (Adriance et al., 2005). As a LE cell turns metastatic, its normal keratin-based epithelial cytoskeleton converts to either mesenchymal or amoeboid-like structure. In a mesenchymal cell, cytoskeleton switches from keratin to vimentin-based composition, which allows it to morph dynamically. Likewise, amoeboid-like metastatic cell completely loses its internal cytoskeletal structural support and deforms like fluid (Zijl, Krupitza, & Mikulits, 2011) . Either way, as the LE cell loses its stiff and regulated keratin-based structural support, it loses homeostatic structure and become extremely deformable.

As for the interactions between the IDC cell and its neighbours, researchers found that when a LE cell turns metastatic, its desmosomes and E-cadherin are down regulated, weakening cell-to-cell adhesion (Zijl, Krupitza, & Mikulits, 2011; Chidgey & Dawson, 2007; Shamir et al., 2014). Adhesion between metastatic cell and ECM also alters due to the downregulation of integrin (Kumar & Weaver, 2009).

A common trait of a migrating metastatic cell is protrusion. A protrusion is an extension of cell membrane in which its end attaches onto another cell or ECM and pulls the metastatic cell (Figure 2.19). In a metastatic cell, the actin filaments, which are responsible for deformation and structural support of cells, deform extensively to form protrusion. The protrusion probes for and attaches onto a surface, either in ECM or cells. The protrusion and stress fibre, the actin fibres in the rear portion of the cell, contracts to pull the cell toward the attached point (Figure 2.19). The protrusion and rear contraction are considered as the main contributor of metastatic cell migration. Figure 2.20f shows the of LE cells extending protrusions in Matrigel. Furthermore, a metastatic cell secretes matrix metalloproteinases (MMPs) that degrade ECM in contact, making it easier to extend protrusions (Zijl et al., 2011).

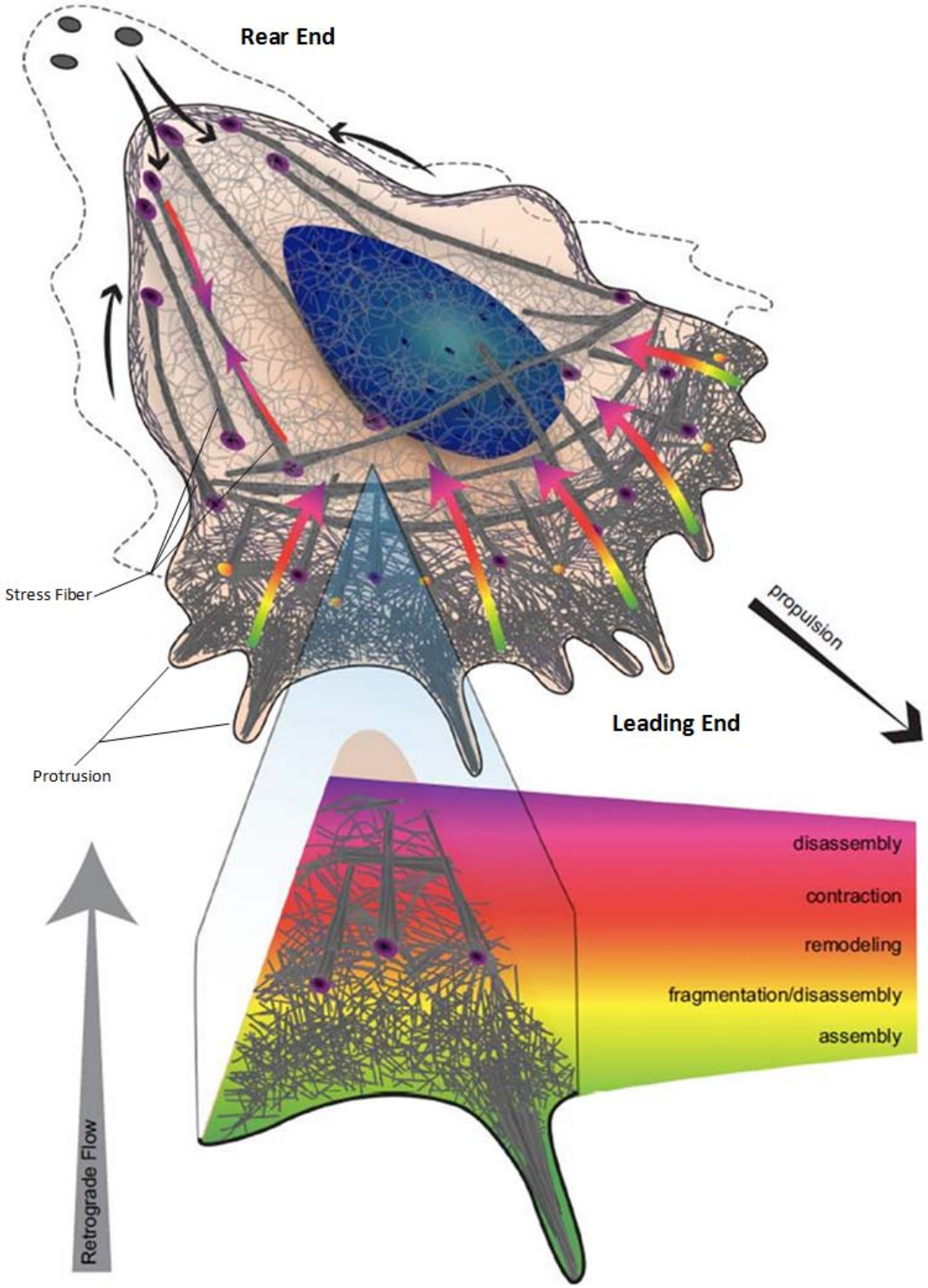

Figure 2.19: Conceptual Drawing of Metastatic Cell with Protrusion and Stress Fibre
(Blanchoin, Boujemaa-Paterski, Sykes, & Plastino, 2014)

Shamir et al. (2014) conducted an experiment to observe the effect of removing E-cadherin and introducing Twist1 to extracted mouse mammary ducts. Twist1 is a protein molecule that binds to the DNA of a LE cell and changes some of its characteristics from those of an epithelial cell to those of a mesenchymal cell (Genetics Home Reference, 2017). In the experiment, mammary ducts of mice were extracted and submerged in Matrigel, an ECM-recapitulating gel substance, to replicate the cell behaviours in actual mammary gland; when the duct extracts are in Matrigel, they rearrange into spheres, in which LE cells are enclosed by ME cells (Figure 2.20). Shamir et al. (2014) observed that the adherence between LE cells weakened the when E-cadherin was removed from LE cells; these cells, however, did not disseminate from the duct (Figure 2.20A-C). Contrarily, the LE cells disseminate from the duct with protrusions when Twist1 is introduced (Figure 2.20D-F).

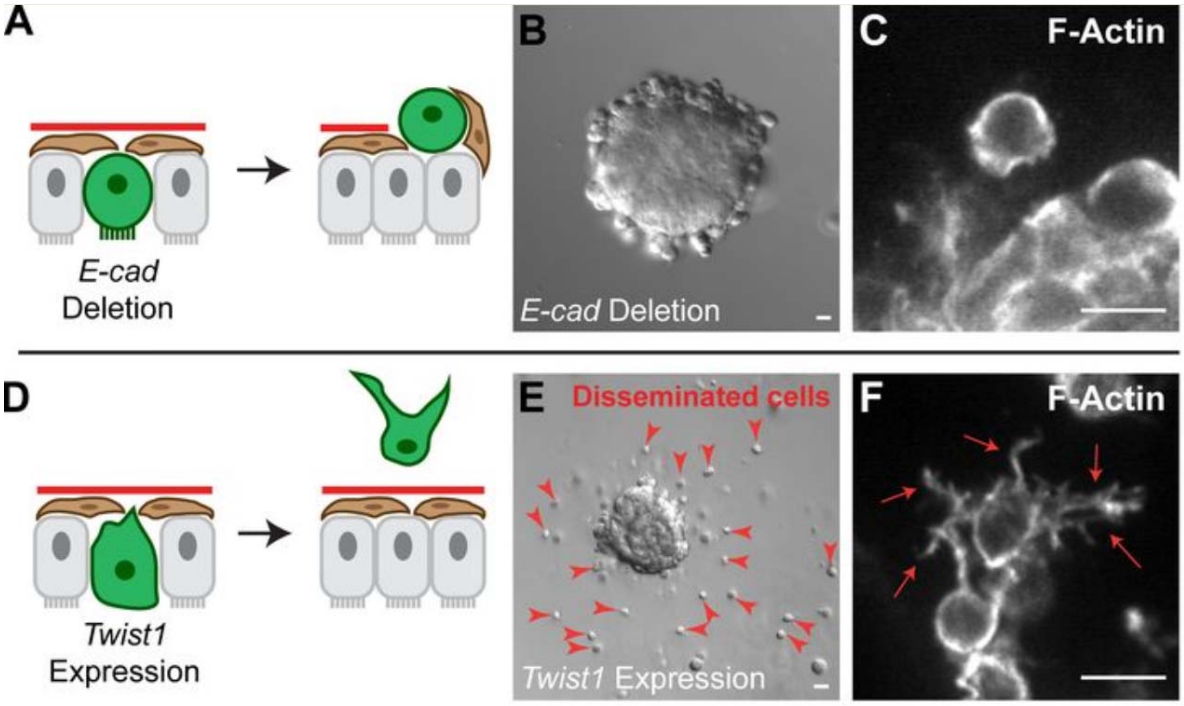

Figure 2.20: Luminal Epithelial Cell of Mouse with E-Cadherin Deletion and Twist1 Introduction
(Shamir et al., 2014)

A metastatic LE cell, relying on drastic internal changes and skewed interactions with its neighbours, breaks through ME cells, a basement membrane layer and ECM so as to begin its deadly metastatic journey (Adriance et al., 2005).

2.3 Modeling of Mammary Duct Development and Metastasis

In recent years, the FE software developed in the Brodland lab has been used to simulate increasingly complex and unique morphological phenomenon, including development of mammary ducts and cancer metastasis. Most of the cell movements and rearrangements they studied are driven primarily by non-uniform assignments of ITs, and this approach is referred to as modified interfacial tension (MIT), where the adjective "modified" refers to fixed values modified from a uniform set of ITs. The software was recently enhanced so that it could recapitulate three distinguishing mechanisms of metastatic and embryonic LE cells to their DITH-based FE software: protrusion, tension gradient and boundary capture. These mechanisms allow an individual cell to gain motility that is not possible by MIT alone. This section presents these nascent features and how they are used in this study to simulate metastatic LE cell escape. The motivation for development of these features is introduced in this section, while comprehensive explanations of them are discussed in the Methodology Chapter.

2.3.1 Metastasis: Protrusion

Brodland and Veldhuis (2012) reviewed the traits of a motile cancer cell, and discussed how they can be incorporated in FE software. They state that that a protrusion provides significant motility to a metastasizing cell by latching onto other elements and contracting. For instance, in Figure 2.21, the protrusion from Cell A penetrates between Cell B and C, and its end latches onto Cell D. The protrusion then retracts and pulls Cell E between D and F, resulting in the intercalation of Cell A between B and C. Brodland and Veldhuis (2012) incorporated this protrusion mechanism by creating a special protrusive interface that exerts a tension γ^P; Figure 2.22 shows a FE model where Cell C creates protrusion

between Cell N's, where the interfacial force of the protrusion, γ^P, is significantly higher than other ITs (Brodland & Veldhuis, 2012).

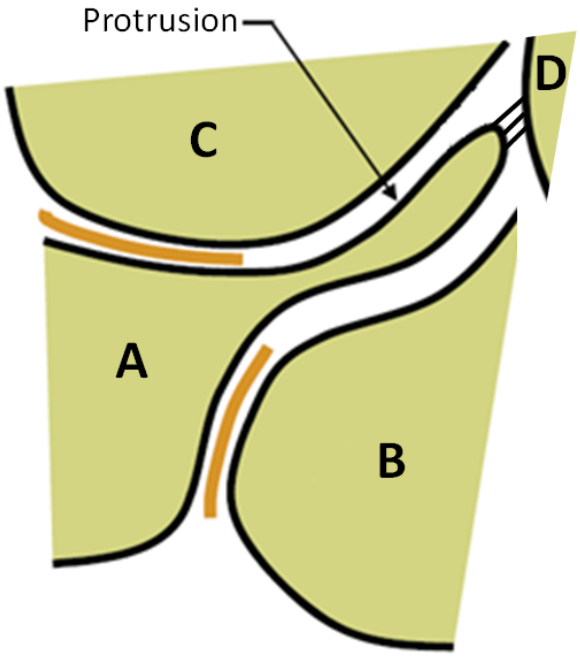

Figure 2.21: Conceptual Drawing of Protrusion of Cell
(Brodland & Veldhuis, 2012)

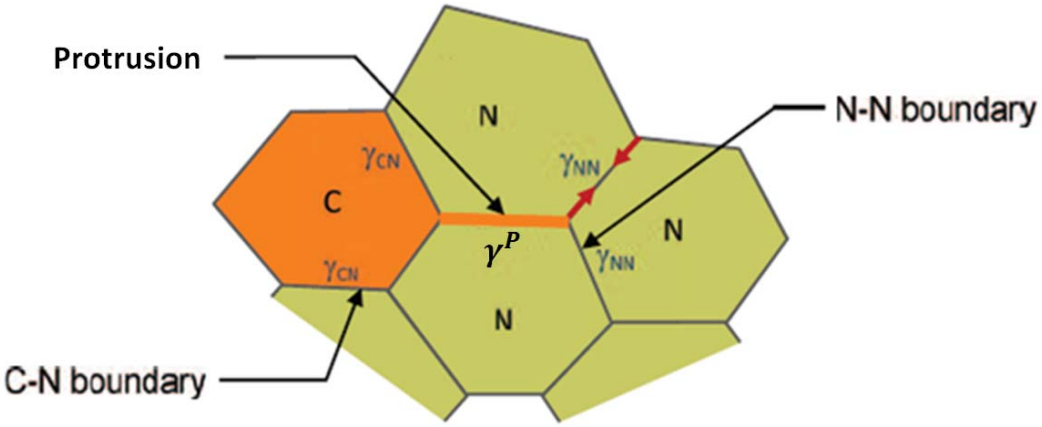

Figure 2.22: Protrusion in DITH-based FE Model
(Brodland & Veldhuis, 2012)

2.3.2 Mammary Duct Development

Neumann at el. (In preparation) corroborated the discovery of the radial intercalations of LE cells driving the mammary duct development with the DITH. The Brodland lab created a FE model of the mouse mammary lob (Figure 2.23) and simulated its development.

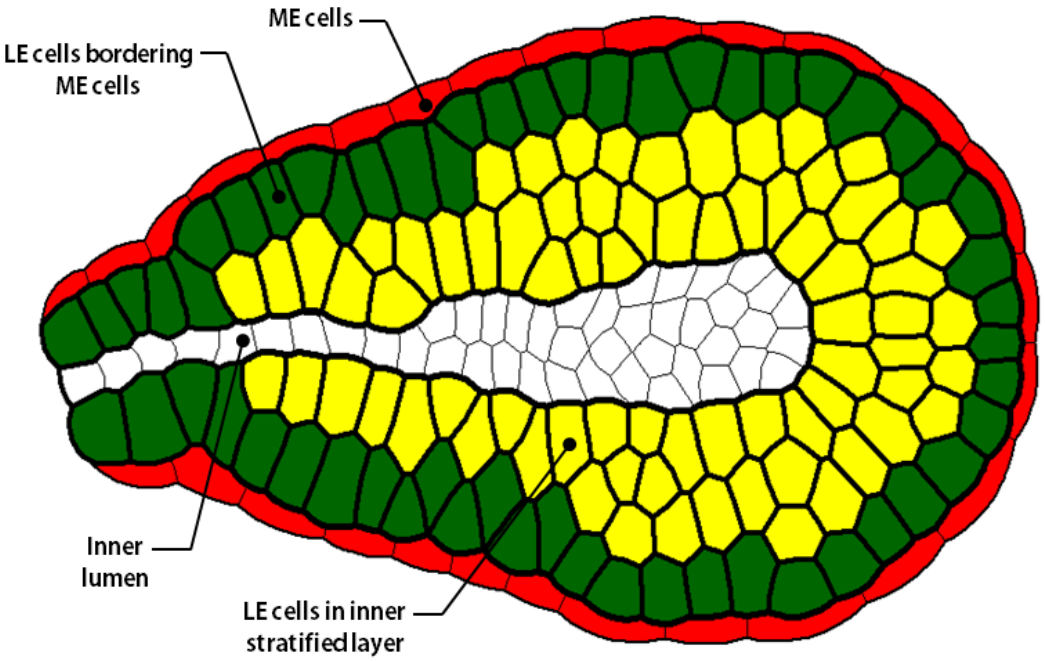

Figure 2.23: DITH-based FE Model of Mammary Duct: Initial Geometry
(Neumann et al., In preparation)

The goal of the simulation was to investigate whether the mammary duct can be formed by radial intercalations such that the LE cells in the lobe (shown yellow) reach and adjoin the outer ME layer to form a bilayer structure. Based on the observations from the numerous trials of in-vitro experiments and FE simulations, Neumann at el. (In preparation) identified three mechanisms that allow a LE cell to successfully intercalate: protrusion, tension gradient and boundary capture.

A protrusion is shown along an interface extending from a LE cell, and its higher tension compared to the other ITs near it is indicated by thicker interface lines in Figure 2.24A (+0f - +4f). It successfully pulls the cell to the ME cell using the mechanisms discussed in Section 2.3.1.

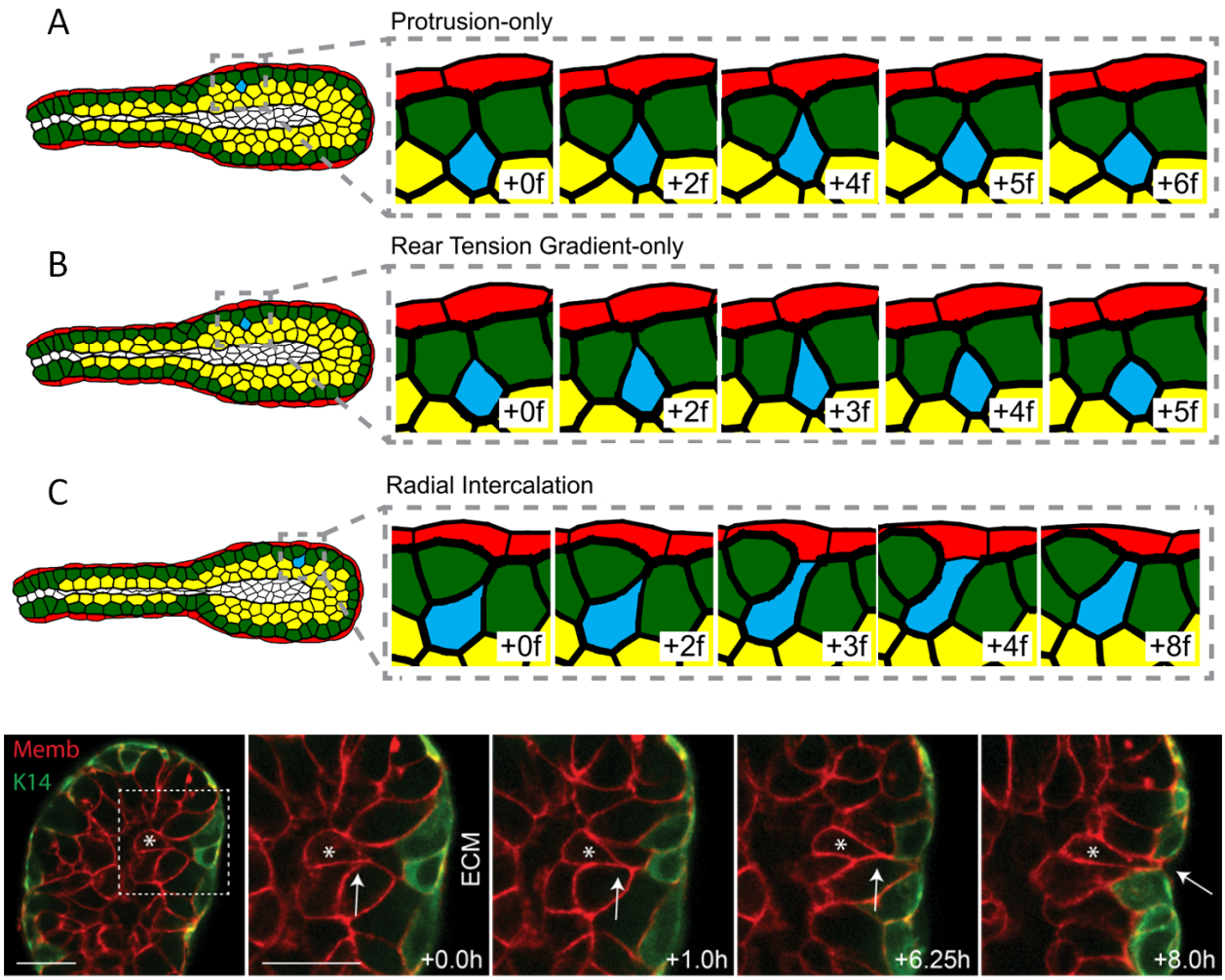

Figure 2.24: Radial Intercalation of LE Cell in DITH-based FE Simulation
(Neumann et al., In preparation)

Another observation made from microscopy is that more actin fibres tend to be present near the posterior end of an intercalating cell, indicating higher contraction levels at the rear of the cell compared to its front portion. The DITH-based FE software captures this mechanism by using a *tension gradient*. When this kind of tension gradient is applied to a cell, its ITs increase from the front to the rear ends, instead of remaining constant based on cell-cell or cell-matrix interface type. +0f of Figure 2.24B illustrates the increase of IT, where the line weight of the interface represents IT strength.

Intercalating cells typically have protrusions that create a sharp front ends, and a tension gradient that forms a smooth curvature at the rear (Krens et al., In preparation). In combination, protrusion and

tension gradient produce intercalating cells shaped like a tear drop as shown in +0f - +2f in Figure 2.24C. Cell microscopy confirms that the majority of intercalating cells are teardrop shaped (Figure 2.24). (Neumann et al., In preparation)

As shown in Figure 2.24A and B, either protrusion, tension gradient or the combination of the two can make LE cells reach the ME layer. However, since all the outer LE cells (green) have the same LE-ME IT, it is not possible to have the intercalating cell's basal edge expand after it contacts the outer cells. Hence, a feature called boundary capture was added, where the tension along the new interface between intercalating LE and ME cells has relatively lower IT than the edges of outer LE and ME cells for a defined period of time. The boundary capture is activated until the intercalating cell has adjoined with ME layer as much as other outer LE cells (Figure 2.24C, 3f - 4f). Then, the IT of the recently intercalated cell returns to the normal LE (Figure 2.24C, +8f).

Neumann et al. (In preparation) found that hoop stress caused by the smooth contractile muscles of ME cells facilitates the formation of bilayered duct architecture, and hence greater elongation. To account for the hoop stress, vertical stress toward the center of the duct is applied to each node. The initial configuration of the model turns into as shown in Figure 2.25 after two sets of hoop stresses were applied. (Neumann et al., In preparation)

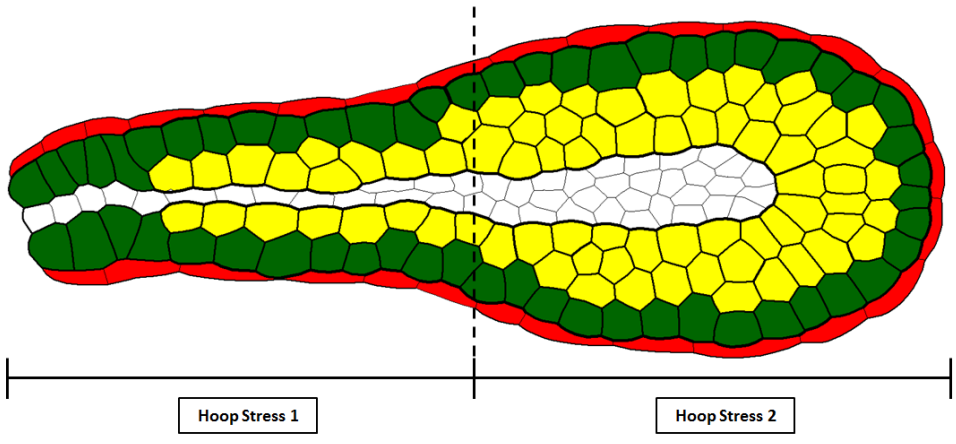

Figure 2.25: Mammary Duct with Hoop Stress
(Neumann et al., In preparation)

Neumann et al. (In preparation) discovered that inner LE cells in the lobe portion have a high rate of proliferation, which supplies the intercalating cells that elongate the duct. These cells proliferate by growing into their mature size and then dividing into two daughter cells. This process was programmed into the FE software, as shown in Figure 2.26; the parent cells divides into half, along its shorter ends, into two daughter cells at 1f. Through 2f to 4f, the daughter cells increase in area until they reach the area of their parent cell.

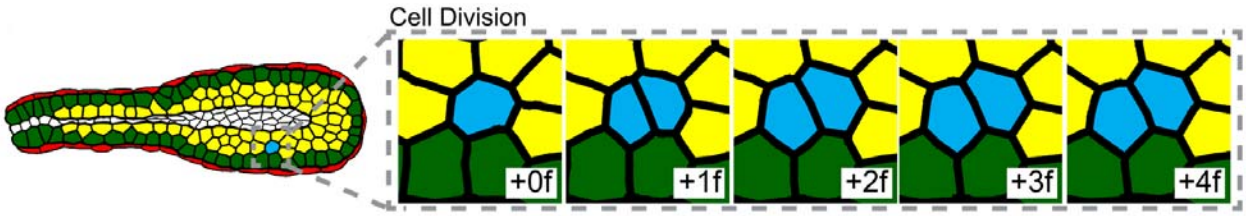

Figure 2.26: Time-lapse Simulation Images of LE Cell Division and Growth
(Neumann et al., In preparation)

Using all of the mechanisms just described, a FE simulation of an elongating duct, as shown Figure 2.27 was carried out (Neumann at el., In preparation).

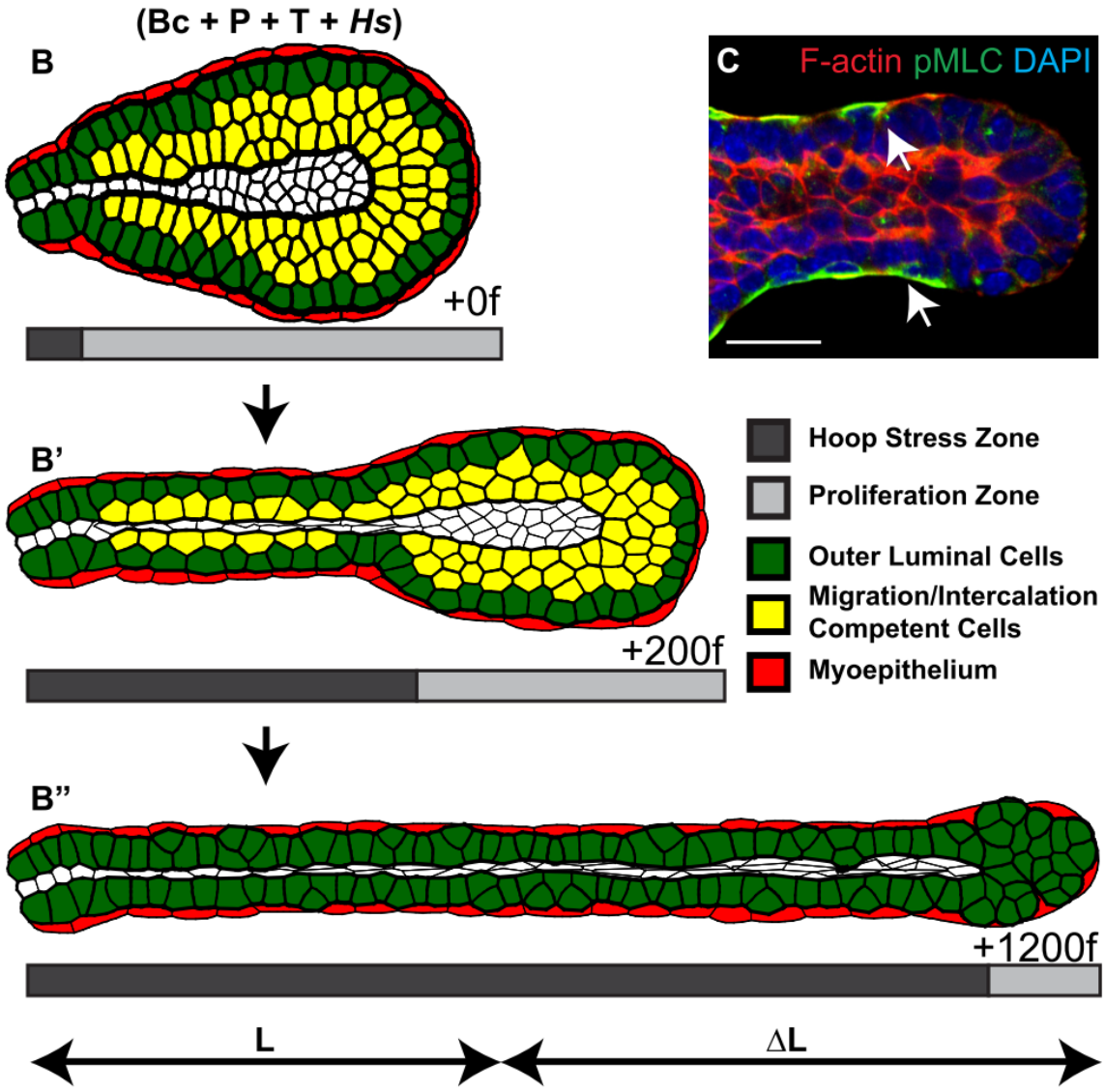

Figure 2.27: DITH-based FE Simulation of a Mammary Duct Development
(Neumann et al., In preparation)

It showed that this small suite of mechanical features is sufficient to recapitulate a wide range of primary features of mammary duct morphogenesis and elongation.

Chapter 3 : Methodology

As noted earlier, the first stage of breast cancer metastasis is the escape of one or more LE cells from the mammary ducts. In the escape, the metastatic cells detach from the mammary duct and migrate through the surrounding ECM. For this to happen, the cell must lose mechanical homeostasis and gain motility through changes in the forces it exerts.

This study evaluated a wide range of known IT force mechanisms for their ability to cause escape of a single LE cell from a mammary duct using FE simulations. This chapter outlines the homeostatic environment. Then one of the homeostatic LE cells is singled out as potentially metastatic, and these various IT mechanisms were applied to it in order to investigate if, how and why the cell escapes. The applied IT mechanisms include modified interfacial tension (MIT), protrusion and tension gradient.

3.1 Homeostatic Model Setup

3.1.1 Geometry, Material & Boundary Conditions

In terms of the geometry, the cross-section of the duct was modelled since the shape and behaviour of the mammary duct are constant throughout its length. The cross-sectional geometry (Figure 3.1) was modelled with reference to representative schematic drawings like Figure 2.14.

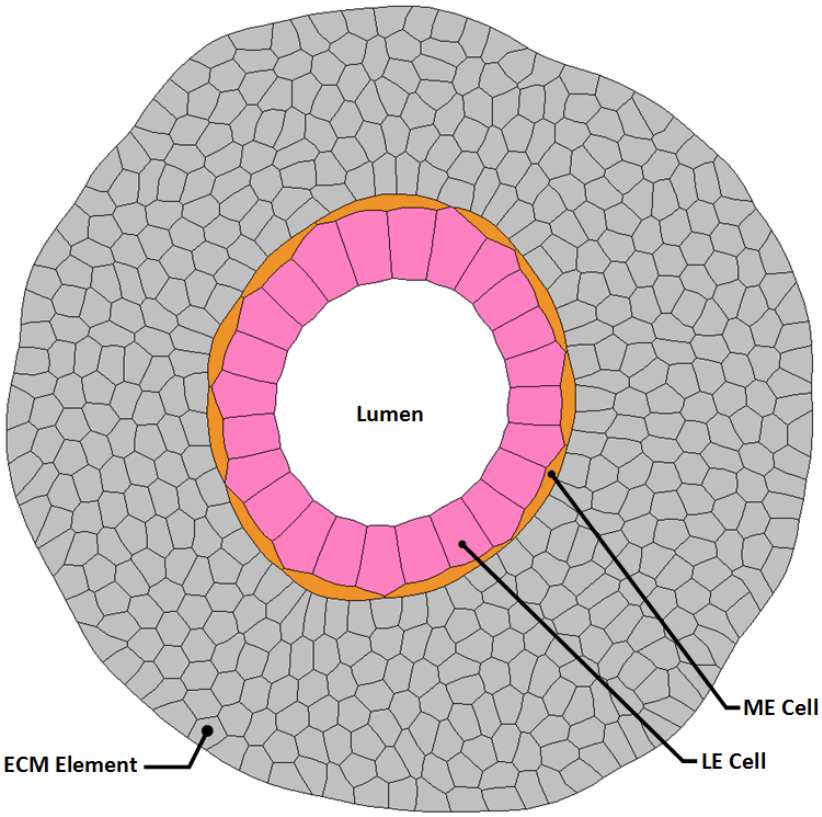

Figure 3.1: Initial DITH-based FE Model Geometry of Homeostatic Mammary Duct: Cross-section

The pink and orange cells represent the LE and ME cells, respectively. The inside of the duct consists of a lumen, which is filled with fluid enriched by milk proteins (Adriance et al., 2005).

Since the scope of this study is the metastatic LE cell's detachment from the duct and migration through ECM, the model includes a zone of ECM that surrounds the duct.

The ECM, which in reality consists of scaffolds of protein fibrils and fibroblasts, was divided into small 'arbitrary elements' to allow the implementation of the protrusion and tension gradient features discussed in Section 2.3. Moreover, the ECM elements were discretized as smaller elements than normal cell sizes to better replicate cell penetration in ECM.

The nodes in the initial configuration were assigned as shown in Figure 3.2. Enough nodes were assigned to the model so that the cells could deform with smooth surface curvatures, as real cells do. All of the dashpots inside the cells were assigned the same value as the true values for LE and ME cells and ECM are not known, and their choice of viscosity values would affect only the time course of the simulations, not their outcomes. The lumen is represented by a single "cell" of fixed area (volume) that has of the order of 20 to 25 interfaces, according to the number of LE cells that surround it.

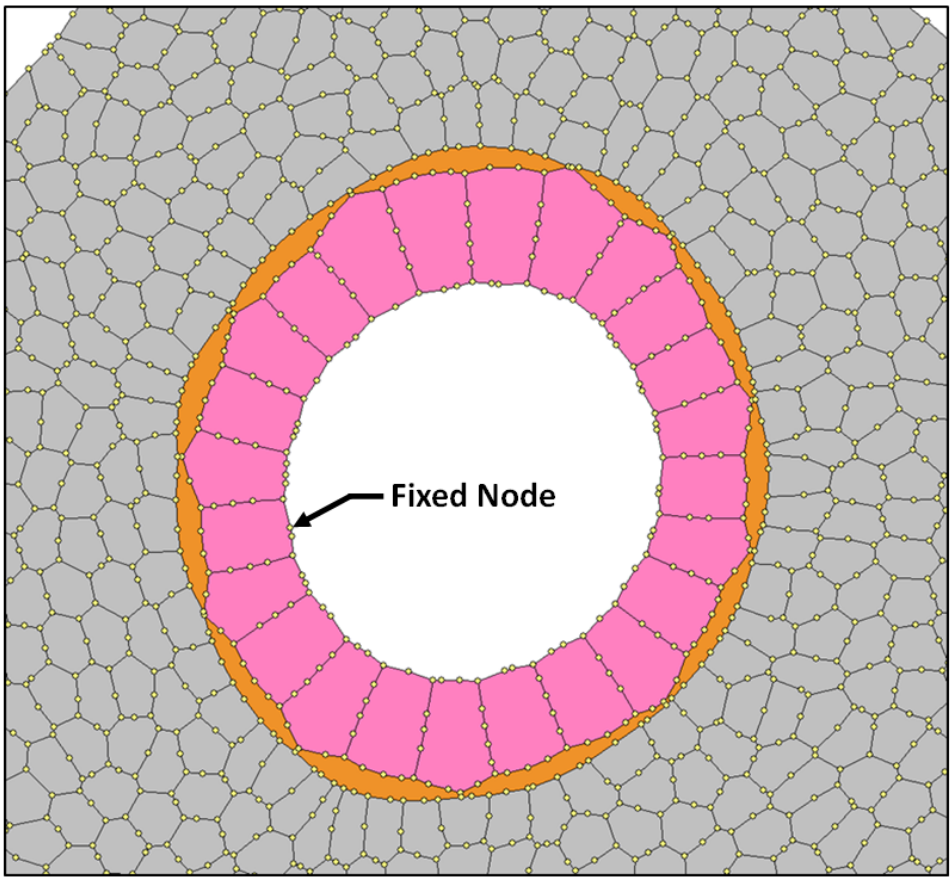

Figure 3.2: Node Placement of Initial Model Geometry

In a finite element model, it is necessary to anchor a certain number of points so that the model does not undergo spurious translations or rotations. This is accomplished by anchoring one node to constrain motion in the x- and y-directions. And the solver automatically finds the solution with minimum rotation about the anchor point. The area (volume) of each cell or other element (ECM or lumen)was set to remain constant; without the area constraint, every element would shrink permanently because every element edges exert tensile forces.

3.1.2 Interfacial Tensions in Homeostatic Cells

Regardless of whether the cells are in homeostasis or dynamic rearrangement, they are constantly exerting ITs. The first step in the analysis was, therefore, to find the combination of ITs that preserve the steady-state homeostatic geometry. This section identifies the IT conditions required to satisfy the homeostasis of the specific initial geometry shown in Figure 3.1.

In the initial geometry, the following types of interfaces are present: Lumen-LE, LE-LE, LE-ME, ME-ME, ME-ECM and ECM-ECM. The interfaces that can potentially appear include Lumen-ME, Lumen-ECM and LE-ECM. The ITs of these interfaces are presented in Table 3.1, where the row and column headers are the bordering elements in contact. For example, γ^{SL} represents the IT of Lumen (row) - LE (column) interface. There is a single virtual "cell" representing the lumen and thus there are no Lumen-Lumen interfaces.

Table 3.1: Interfacial Tension Parameters: Homeostasis

Lumen	LE	ME	ECM	Adjoining Elements
Not Applicable	$\gamma^{Lumen-LE}$	$\gamma^{Lumen-ME}$	$\gamma^{Lumen-ECM}$	**Lumen**
	γ^{LE-LE}	γ^{LE-ME}	γ^{LE-ECM}	**LE**
		γ^{ME-ME}	γ^{ME-ECM}	**ME**
			$\gamma^{ECM-ECM}$	**ECM**

By conducting multiple trials with various combinations ITs, and informed by CellFIT-inspired (Brodland et al., 2014; Hiiragi, Veldhuis, Ehsandar, Cox, & Brodland, 2017) TJ angle analyses, the following IT conditions were deduced as necessary to maintain the homeostasis of the mammary duct:

1. **a.** $\boldsymbol{\gamma^{ME-ME} << \left(\gamma^{ME-ECM1} + \gamma^{ME-ECM2}\right)_{ME-ME\ axis}}$

   b. $\boldsymbol{\gamma^{ME-ME} << \left(\gamma^{ME-LE1} + \gamma^{ME-LE2}\right)_{ME-ME\ axis}}$

   The outer TJs of ME-ME interfaces join one ME-ME and two ME-ECM edges, and the inner join one ME-ME and two ME-LE edges. A ME-ME interface is almost perpendicular to other edges at both inner and outer TJ; to maintain such geometry, γ^{ME-ME} must be significantly lower than the γ^{ME-ECM} and γ^{ME-LE}. The closer γ^{ME-ME} is to the sum of the other ITs in the axis of ME-ME edge, the shorter the ME-ME interface become; if γ^{ME-ME} becomes greater, the ME-ME interfaces will shorten until the ME-ME TJs undergo neighbour changes and expose LE cells to ECM. Furthermore, γ^{ME-ME} must be very low because the ME-ME interfaces are short; a little magnitude of γ^{ME-ME} can pull in the ME-ME TJs and cause neighbour change (Figure 3.3 +0f - +2f).

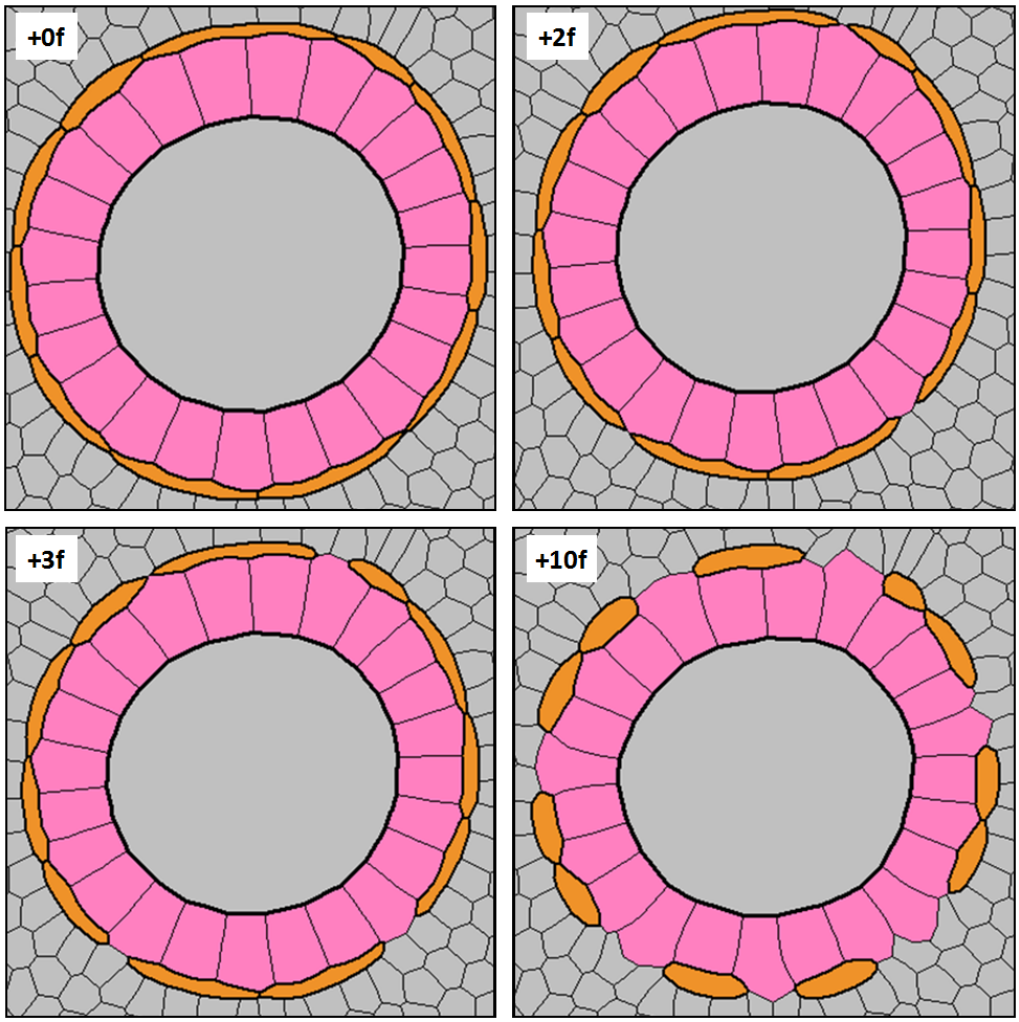

Figure 3.3: Luminal Epithelial Cells Coming into Contact with the ECM

2. $\boldsymbol{\gamma^{LE-ECM} > \left(\gamma^{ME-ECM} + \gamma^{LE-ME}\right)_{LE-ECM\ axis}}$

This condition is required for the LE cells to come into contact with the ECM. Because the ME-ME interfaces are short at the starting configuration, even if Condition 1 is satisfied, the dashpot forces may bring ME-ME TJs closer and cause the neighbour change.

Condition 2 is needed to prevent the LE-ECM interface from expanding after the neighbour changes. Sufficiently strong γ^{LE-ECM} pulls the LE-ECM TJs inward, which would then lead to another neighbour change, which would reinstate the ME-ME interface. Without Condition 2, the LE cells continue to reveal to ECM as shown in +3f to +10f in Figure 3.3.

3. a. $\boldsymbol{\gamma^{LE-LE} < \left(\gamma^{LE-ME1} + \gamma^{LE-ME2}\right)_{LE-LE\ axis}}$

   b. $\boldsymbol{\gamma^{LE-LE} < \left(\gamma^{Lumen-LE1} + \gamma^{Lumen-LE2}\right)_{LE-LE\ axis}}$

   The outer TJs of LE-LE interfaces join one LE-LE and two LE-ME interfaces, while the inner join one LE-LE and two Lumen-LE interfaces. The inner and outer LE-LE edges are almost perpendicular to LE-ME and Luminal-LE edges in the homeostatic geometry; to maintain such a geometry, γ^{LE-LE} must be significantly lower than the γ^{LE-ME} and $\gamma^{Lumen-LE}$. The closer γ^{LE-LE} is to the sum of the other ITs in the axis of LE-LE edge, the shorter the LE-LE interface becomes and other edges angularly narrow. If γ^{LE-LE}exceeds the sum of the other ITs in LE-LE axes in every time step, the LE-LE interfaces will shrink and undergo neighbour changes, creating ME-Lumen interfaces thus.

4. $\boldsymbol{\gamma^{ECM-ECM} \cong 0.5}$

   The surrounding ECM has been meshed into elements to simulate the migration of the metastatic cell. Although the ECM consists of cells such as fibroblasts, a large portion of it is filled with intertwined protein fibrils and fluid. As the DITH currently only support cell-cell or cell-matrix interaction, it is difficult to quantify the ITs of these arbitrary ECM element interfaces. However, when $\gamma^{ECM-ECM} = 0,$ a metastatic cell with protrusion cannot advance in ECM because it only pulls in the ECM nodes. Therefore, $\gamma^{ECM-ECM}$ was set to 0.5 as an arbitrary IT that represents the stiffness of the ECM, which is sufficiently high to provide stiffness for a metastatic cell with protrusion can pull itself past ECM.

The rest of the variables, including $\gamma^{Lumen-ME}$ and $\gamma^{Lumen-ECM}$, were not necessary for homeostasis; because the five conditions are satisfied, these interfaces will not arise during the simulation. A modest range of IT values are possible under the constraints outlined in the conditions. And here we choose the

values shown in Table 3.2. These values are generally consistent with those that a CellFIT (Brodland et al., 2014; Hiiragi, Veldhuis, Ehsandar, Cox, & Brodland, 2017) analysis would produce.

Table 3.2: Interfacial Tension Values: Homeostasis

Lumen	LE	ME	ECM	Adjoining Elements
NA	1	NA	NA	**Lumen**
	0.5	1	3	**LE**
		0.1	1	**ME**
			0.5	**ECM**

3.2 Implementing Mechanisms of Single Luminal Epithelial Cell Escape

After creating the homeostatic model, an arbitrary LE cell was converted to an "escape" (Esc) cell, as shown in Figure 3.4.

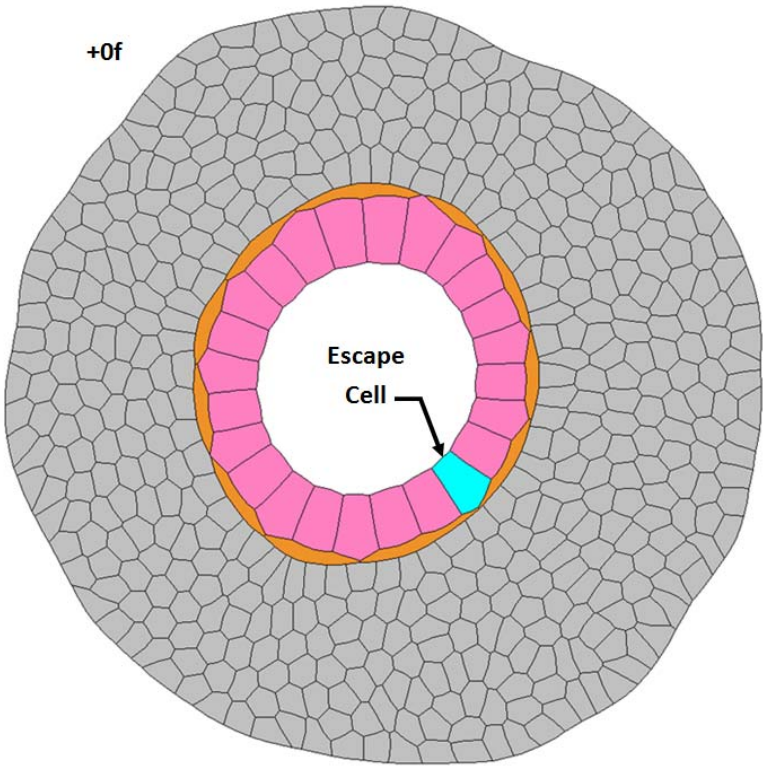

Figure 3.4: Initial Model Geometry of Single Luminal Cell Escape

The Esc cell must achieve two actions to successfully escape: detachment from the duct, and continuous migration through the ECM. The mechanisms explored in this study are MIT, protrusion and tension gradient. Parametric analyses of individual and combinations of these mechanisms were conducted to examine their effects on the detachment and ECM migration of the Esc cell.

3.2.2 Modified Interfacial Tension

In homeostasis, the IT of every interface stays fairly constant; therefore the nodes remain in steady-state and cells static. This implies that one or more changes in ITs must be introduced in order to cause any displacements of nodes and deformations of cells. In MIT, the Esc cell is assumed to change its interfacial interactions with its surrounding elements, thus causing the change in ITs. As soon as the ITs of one or more edges change, the nodes displace until they achieve a new steady-state. The first mechanism considered is MIT, and the homeostatic combinations of ITs were modified to determine if doing so was sufficient to produce Esc cell escape.

With the addition of the Esc cell type, there are five more IT parameters present in the model, as shown in Table 3.3.

Table 3.3: Interfacial Tension Parameters: Single Cell Escape

Lumen	Escape	LE	ME	ECM	Adjoining Elements
NA	$\gamma^{Lumen-Esc}$	$\gamma^{Lumen-LE}$	$\gamma^{Lumen-ME}$	$\gamma^{Lumen-ECM}$	**Lumen**
	NA	γ^{Esc-LE}	γ^{Esc-ME}	$\gamma^{Esc-ECM}$	**Escape**
		γ^{LE-LE}	γ^{LE-ME}	γ^{LE-ECM}	**LE**
			γ^{ME-ME}	γ^{ME-ECM}	**ME**
				$\gamma^{ECM-ECM}$	**ECM**

The objective of MIT is not to identify the exact values of the ITs that drive the cell escape; the numbers of combinations of ITs of cell escape are infinite, and there are no experimental data that can empirically verify which of those are correct. One can use MIT, however, to find the conditions that the combination

of ITs must satisfy for the Esc cell to escape, just as how the IT conditions were found for homeostasis in Section 3.1.2.

3.2.1 Reactivation of Radial Intercalation Mechanisms

The protrusion and tension gradient features introduced in Section 2.3 are applied to simulate the single cell escape. Unlike MIT, where ITs depend on the type of cell-cell and cell-matrix interfaces, these mechanisms are applied to the Esc cell independently, and thus the homeostatic ITs from Table 3.2 are maintained.

3.2.1.1 Protrusion

Another possible escape mechanism is protrusion action, and when a protrusion feature turns on, the FE software extends one protrusion from the Esc cell, which has a special IT γ^P (Figure 3.5). As the objective of the simulation is to detach the Esc cell from the mammary gland, the software chooses the interface that points most strongly away from the duct as the location of the protrusion. The direction is calculated by constructing the shortest vector from the centroid of the Esc cell to the outer edge of the ECM in the model, which is the outer ECM perimeter. The software then selects one of the edges extending from the Esc cell TJs that is oriented closest to the found direction. Once the edge is selected, the protrusion extends from the TJ of the edge to the next TJ; In Figure 3.5, a new protrusion is formed at +0f, extending from TJ A to D.

If a protrusion has a sufficiently strong IT that it shortens beyond the minimum node distance, the software will assign a new protrusion upon neighbour change using the aforementioned selection process. Figure 3.5 shows the instance of a protrusion strong enough to shorten until neighbour change; the interface ABCD shortens and undergoes ENR until TJ A and D are left through +0f to +75f. The neighbour change at +86f replaces node A and D with A' and D', and the new protrusion is formed from TJ A'to E'. The protrusion feature continues until the Esc cell reaches the outer bound.

The only parameter of protrusion is its IT strength, γ^P. Multiple simulations were conducted with increasing γ^P starting from 0.5 (= $\gamma^{ECM-ECM}$) to observe its effect on the Esc cell escape. The range of parameters explored were based on previous lamellipodium studies (Brodland & Veldhuis, 2006; Brodland & Veldhuis, 2012).

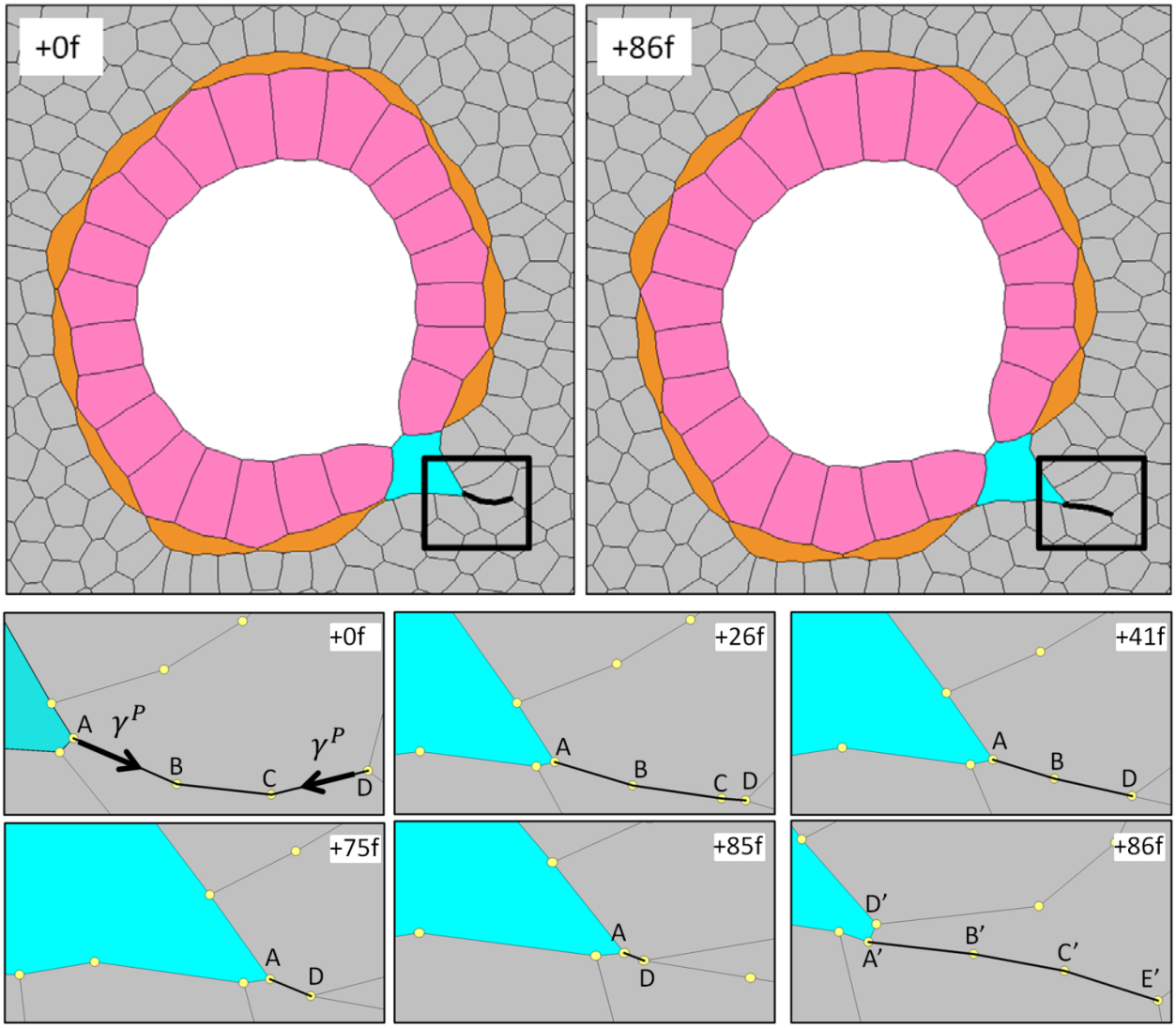

Figure 3.5: Time-lapse Images Demonstrating Protrusion

Stress Fibre

Stress fibres were also incorporated into the model to retract the rear portion of a protruding cell (Figure 2.19). Without stress fibre Esc cells with high protrusion strengths can stretch to biologically unrealistic high aspect ratios, as shown in Figure 3.6a. To replicate the rear retracting stress fibre introduced in Section 2.3.1. The FE software computes the aspect ratio of the Esc cell at every time step by drawing the best fitting ellipse of the cell and dividing the longer length by the shorter width. As soon as the aspect ratio exceeds the set limit (typically >1.5), the stress fibre applies forces to every nodes of Esc cell, in the long axis of the cell and toward the centre of the cell to make the aspect ratio more realistic. The strength of stress fibre is linearly proportional to the aspect ratio; if the Esc cell continues to stretch and increase in aspect ratio, the stress fibre forces applied to the nodes become stronger. The Esc cell in Figure 3.6b consists of stress fibres that activates beyond the aspect ratio of 2.

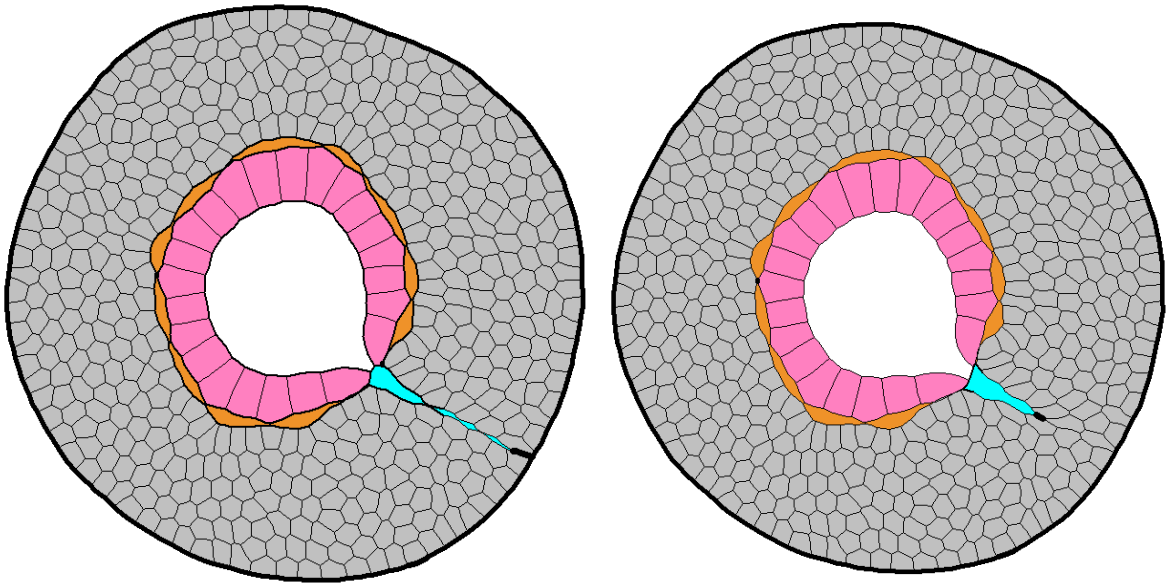

a. Without stress fibre b. With stress fibre

Figure 3.6: Escape Cell with Protrusion: with (a) and without (b) Stress Fibre

3.2.1.2 Tension Gradient

When a tension gradient is assigned to an Esc cell, its IT increases from the front to the rear end. The software constructs the best fit ellipse of the Esc cell. The long axis of the ellipse aligns with the aforementioned vector from the centroid of the cell to the closes outer edge of the ECM in the model; and the more outward end of the ellipse is referred to as front, and inward edge the rear. The tension gradient feature includes two parameters: mean strength and the degree of gradation. The mean strength is the IT of the edges along the centroid of the ellipse, and the IT of the front and rear end is increased or decreased by the degree of gradation. The tension gradient IT increases linearly from the front to rear end along the long axis of the ellipse. The IT of each edge is assigned based on the location of its centre along the long axis of the best-fit ellipse.

In Figure 3.7, the Esc cell is assigned tension gradient. The magnitudes of mean strength and degree of gradation are 1 and 0.7, and thus the Esc cell's front, middle and rear ITs are 0.3, 1 and 1.7, respectively. All the Esc cell nodes displace toward the rear end since the edges closer to the rear consist of higher ITs. As a result, the edges near the front undergo ENA (+37f - +38f) and rear ENR (+75f - +76f). In the figures, the strength of the tension along any particular cell edge is indicated by the line thickness used to draw that interface. The tension along any given edge is set to be uniform from one edge node to the next, but changes from one edge segment to the next around the perimeter of the Esc cell.

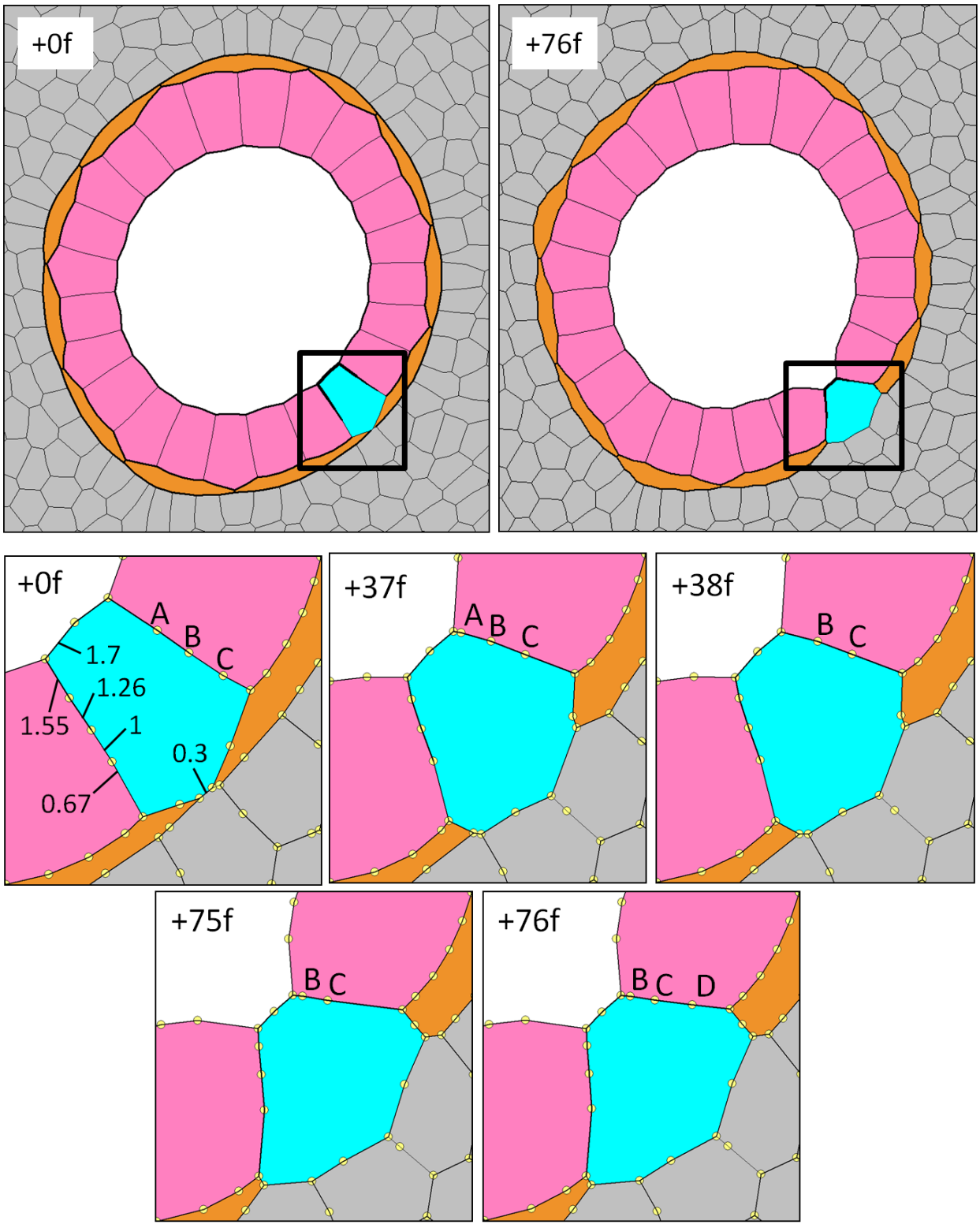

Figure 3.7: Time-lapse Images Demonstrating Tension Gradient (Mean Strength = 1, Degree of Gradation = 0.07)

A parametric study was conducted with varying mean strengths (0.5 – 3) and degrees of gradation (0 – 1) to observe their effects on the Esc cell and to assess their possible capacity to produce escape.

3.2.2.3 Combination of Protrusion and Tension Gradient

Neumann et al. (In preparation) state that either protrusion or tension gradient alone is sufficient to intercalate a LE cell to the ME layer based on FE simulations. During the mouse duct experiment, however, they observed that intercalating LE cells relied on both mechanisms. Therefore a parametric analyses of combinations of MIT, protrusion and tension gradient was also conducted.

3.2.2.4 Boundary Capture, Hoop Stress, Mitosis, Lumen Expansion

Boundary capture is one of the intercalation mechanisms found necessary for the development of a mammary duct because it enables the LE cells to remain in contact to the ME layer. However, applying boundary capture in the metastasis simulations does not facilitate but rather hinder cell escape. The user can choose whether any particular element type activates boundary capture; and for studies of mammary duct development it was needed for the ME cells. For Esc cell, any attachment of the cell to any type of element is not desirable, except for secondary sites or blood vessels (Brodland & Veldhuis, 2012), which are beyond the scope of the prepared model.

Hoop stress, proliferation of epithelial cells and lumen expansion were not considered in this study since the scope of this project focuses on the single cell escape. These two mechanisms act on the entire duct cross-section, whereas the scope of this research is on the escape of a single cell based on the change its individual property.

Chapter 4 : Results

This chapter discusses the findings of several thousand individual simulations. The result is an understanding of if and how various mechanisms (MIT, protrusion and tension gradient) and combinations of same are deemed to be active. This chapter reports the findings of parametric studies proposed in the Methodology, and its last section discusses their biological implications.

4.1 Modified Interfacial Tension

Numerous trial simulations were attempted to identify the combinations of ITs needed to cause the Esc cell to detach from the duct. These studies showed that the Esc cell's ITs must satisfy the following conditions for detachment:

1. **a.** $\boldsymbol{\gamma^{ME-ME} > \left(\gamma^{ME-ECM1} + \gamma^{ME-ECM2}\right)_{ME-ME\ axis}}$

   b. $\boldsymbol{\gamma^{ME-ME} > \left(\gamma^{ME-LE1} + \gamma^{ME-LE2}\right)_{ME-ME\ axis}}$

   (Only for ME-ME interfaces adjacent to the Esc Cell)

   During homeostasis, γ^{ME-ME} has to be almost non-existent to keep the luminal cells enclosed. Conversely, the interface adjoining myoepithelial cells that are enclosing Esc cell must shorten to zero length for the Esc cell to escape. Increasing γ^{ME-ME} tends to shorten the interface between myoepithelial cells that connect the Esc cell and the ECM, and reveals the Esc cell to the ECM through the neighbour change (Figure 4.1, +1f).

2. **a.** $\boldsymbol{\gamma^{Esc-ME} > \left(\gamma^{ME-ECM} + \gamma^{Esc-ECM}\right)_{Esc-ME\ axis}}$

b. $\boldsymbol{\gamma^{Esc-LE} > \left(\gamma^{LE-ME} + \gamma^{Esc-ME}\right)_{Esc-LE\ axis}}$

c. $\boldsymbol{\gamma^{Esc-Lumen} > \left(\gamma^{LE-Lumen} + \gamma^{Esc-LE}\right)_{Esc-Lumen\ axis}}$

An Esc cell-ECM interface is established as the adjacent ME-ME interface shortens and undergoes neighbour change. For the Esc cell to successfully escape, it has to detach from its adjacent LE cells and ME cells and the lumen. The detachment is possible only when the following cell-to-cell contacts are removed: Esc-Lumen, Esc-LE, Esc-ME interfaces. These interfaces must consist of sufficiently strong ITs in order to pull in the TJs and have them undergo neighbour changes; therefore this Condition 2 is also required for Esc cell detachment. The process of the detachment of the Esc cell via MIT is illustrated in Figure 4.1. The +0f and +1f close-ups of Figure 4.1 show the ITs acting on the Esc cell's TJs.

For the Esc-LE interface to shorten and give the Esc cell access to the ECM, Condition 2a, where γ^{Esc-ME} is greater than the combination of γ^{ME-ECM} and $\gamma^{Esc-ECM}$ along Esc-ME axis, must be satisfied. The same concept applies to Condition 2b and 2c that shortens the Esc-LE and Esc-lumen interfaces.

Notice that the ITs on the left side of Condition 2b and 2c are greater than the ITs of previous conditions (e.g., γ^{Esc-LE} in 2b greater than γ^{Esc-ME} from 2a, and γ^{Esc-LE} in 2c is greater than γ^{Esc-LE}). Therefore, the ITs of the Esc increase incrementally toward its rear end as their interface types change. The TJs displace toward the rear end of the Esc cell, and after the series of neighbour changes, the Esc successfully detaches from the duct elements (+50f).

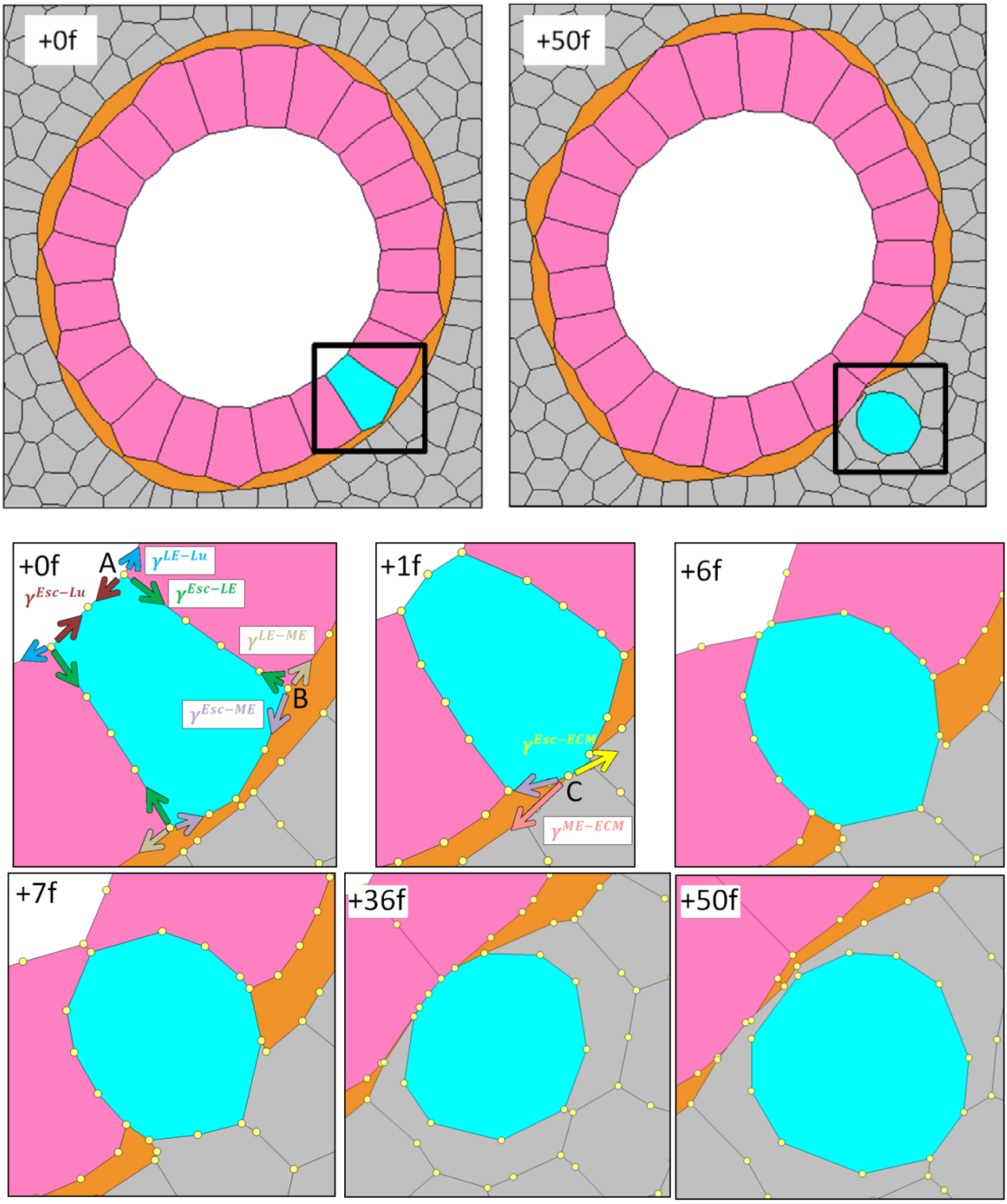

Figure 4.1: Detachment of Escape Cell due to Modified Interfacial Tension Only

Based on the trials, the following combinations of the ITs were found sufficient to drive the Esc cell IT detachment.

Table 4.1. Interfacial Tension Values: Single-Cell Escape

Lumen	Escape	LE	ME	ECM	Adjoining Elements
NA	**4.6**	1	NA	NA	**Lumen**
	NA	**3.2**	**2.2**	**1**	**Escape**
		0.5	1	3	**LE**
			0.1	1	**ME**
				0.5	**ECM**

Unlike homeostasis, where the ITs must be balanced to maintain cell contact of cells, in the cell escape, some ITs must change and be significantly greater or lower than others in order to eliminate certain kinds of interfaces.

Furthermore, a parametric analysis of MIT was conducted by proportionally increasing the left hand side of IT variables of Condition 2 a, b and c: γ^{Esc-ME}, γ^{Esc-LE} and $\gamma^{Lumen-Esc}$. These three ITs were increased by a multiplier factor ranging incrementally from 0.5 to 2 by 0.1. The detachment time of the Esc cell corresponding to the multiplier is show in Figure 4.2.

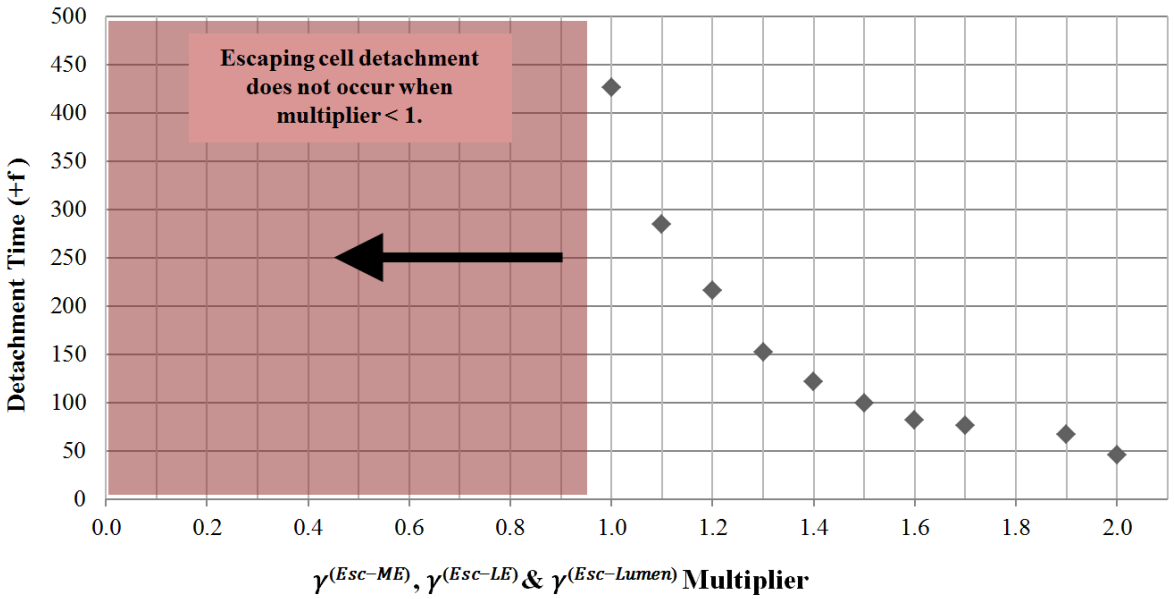

Figure 4.2: MIT Multiplier vs Detachment Time of Escape Cell

As the multiplier increases, the detachment time of Esc cell reduces but the rate of reduction becomes less pronounced at higher multiplier values. The main reason for this is because the ratios between the ITs on the left and right side of Condition 2b and 2c increase less after each incremental increase of the multiplier.

Figures 4.3 and 4.4 show two cases of simulations where the Esc cell detached from the duct and was surrounded by the ECM elements only; an insight from these figures is that the duct is disfigured in 4.4 but has reorganized in 4.3. These distinguishing rearrangements of duct elements after the Esc cell detachment arise depending on the strengths of $\gamma^{Lumen-Esc}$ compared to γ^{Esc-ME} and γ^{Esc-LE}. When $\gamma^{Lumen-Esc}$ is strong enough that the Lumen-Esc interface undergoes neighbour change and the LE-LE contact is established, the duct regains its homeostatic structure after the detachment as shown in Figure 4.3. Conversely, when γ^{Esc-ME} and γ^{Esc-LE} are strong enough that Esc-ME and Esc-LE interfaces undergo neighbour changes first, the Esc cell remains in contact with the lumen and ECM; the ECM then engulfs the Esc cell as $\gamma^{Lumen-Esc}$is greater than $\gamma^{Esc-ECM}$. The result is the disfigured geometry of the duct, in Figure 4.4.

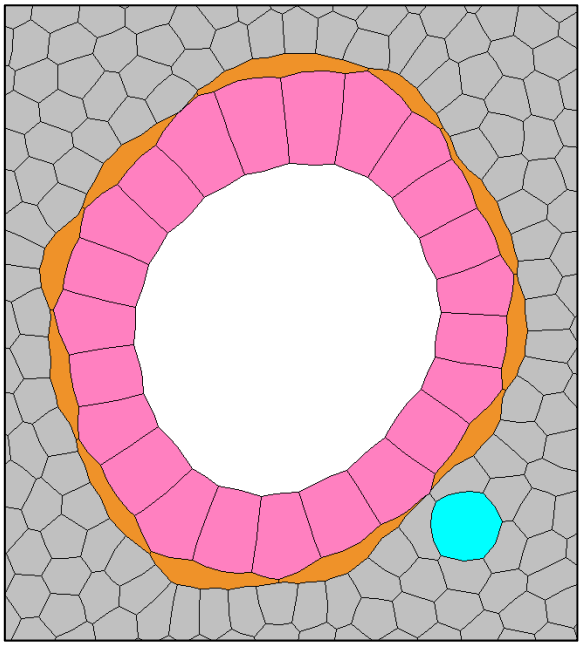

Figure 4.3: Escape Cell Duct Restored after Detachment

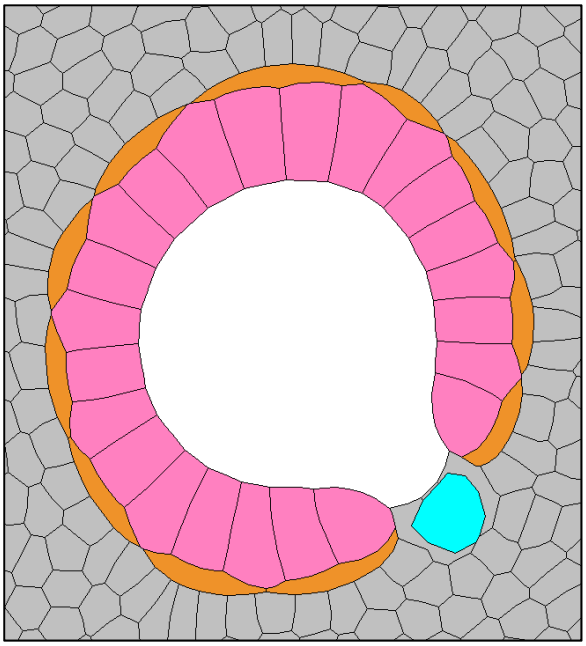

Figure 4.4: Escape Cell Duct Disfigured after Detachment

Once the Esc cell detaches from the duct, it is surrounded by the ECM and $\gamma^{Esc-ECM}$ is applied throughout the Esc cell perimeter. The external forces applied to the Esc cell are $\gamma^{ECM-ECM}$ generated by ECM-ECM edges in contact with the Esc cell. The ratio between $\gamma^{Esc-ECM}$ and $\gamma^{ECM-ECM}$ dictates the circularity of Esc cell; higher $\gamma^{Esc-ECM}$ relative to $\gamma^{ECM-ECM}$ yields more circular and smooth Esc cell shape. All the ECM elements have the same areas and are uniformly placed in the model. Hence soon after the Esc cell detaches and is surrounded by the ECM elements, the ECM-ECM edges pull the Esc cell from all directions, and it cannot further advance in any direction.

4.2 Protrusion

To investigate the potential of protrusions to cause LE cell escape, the Esc cell was assigned protrusions with γ^{P} ranging from 0.5 to 3 (Brodland & Veldhuis, 2012). At the beginning of the simulations, the first protrusions along the ME-ME interface extend from the Esc cell. As the protrusion strengths are greater than a γ^{ME-ME} of 0.1, the ME-ME-protrusion quickly shortens and produces neighbour change, exposing the Esc cell to the ECM. Afterward, all protrusions are formed along ECM-ECM interfaces. When $\gamma^{P} \geq 1$, which exceeds twice the $\gamma^{ECM-ECM}$, the protrusions are strong enough to shorten and consistently produce neighbour change.

However, it was found that protrusions alone are not a sufficient to detach the Esc cell from the duct. Although the protrusion pulls the leading TJ outward, the Esc cell remains in contact with other elements due to its unchanged homeostatic ITs. The protrusion was not tested with γ^{P} greater than 3, as it is physiologically not realistic for one IT to more than thrice the rest of the ITs (Krens et al., In preparation).

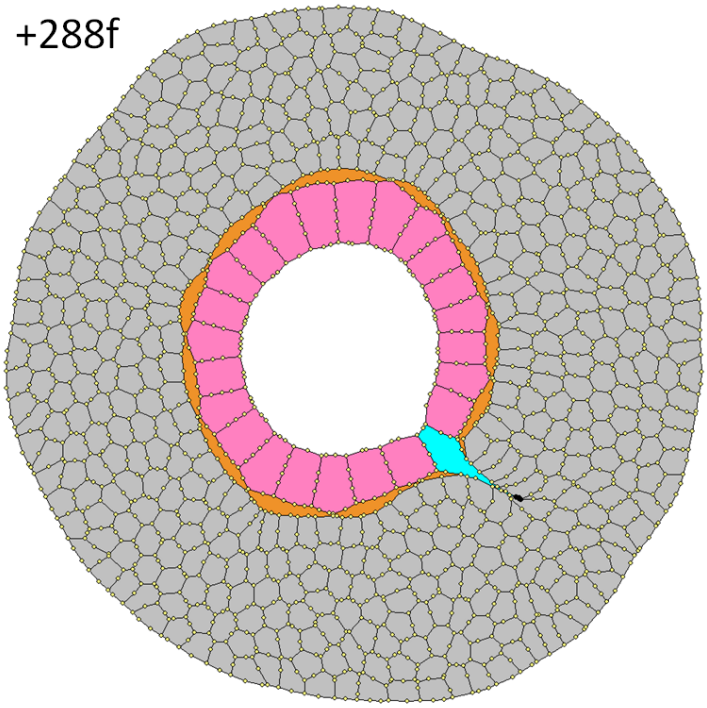

Figure 4.5: Typical Simulation Result of Cell Escape with Protrusion Only ($\gamma^{P} = 1.5$)

To test the effect of protrusions on Esc cell migration in the ECM, it was applied to the steady-state Esc cell surrounded by the ECM after MIT detachment (Figure 4.1, +50f). It was found through trials that that the Esc cell requires protrusions with γ^{P} greater than 1, which is twice $\gamma^{ECM-ECM}$, to successfully migrate through the ECM. The protrusion pulls the Esc cell but requires stress fibre action to control cell aspect ratio. Additionally, every time a protrusion interface shortens and disappear, one extra TJ joins the Esc cell. As the Esc cell moves toward the outer bound, the Esc cell TJs are driven toward the rear end and undergo neighbour changes (Figure 4.6).

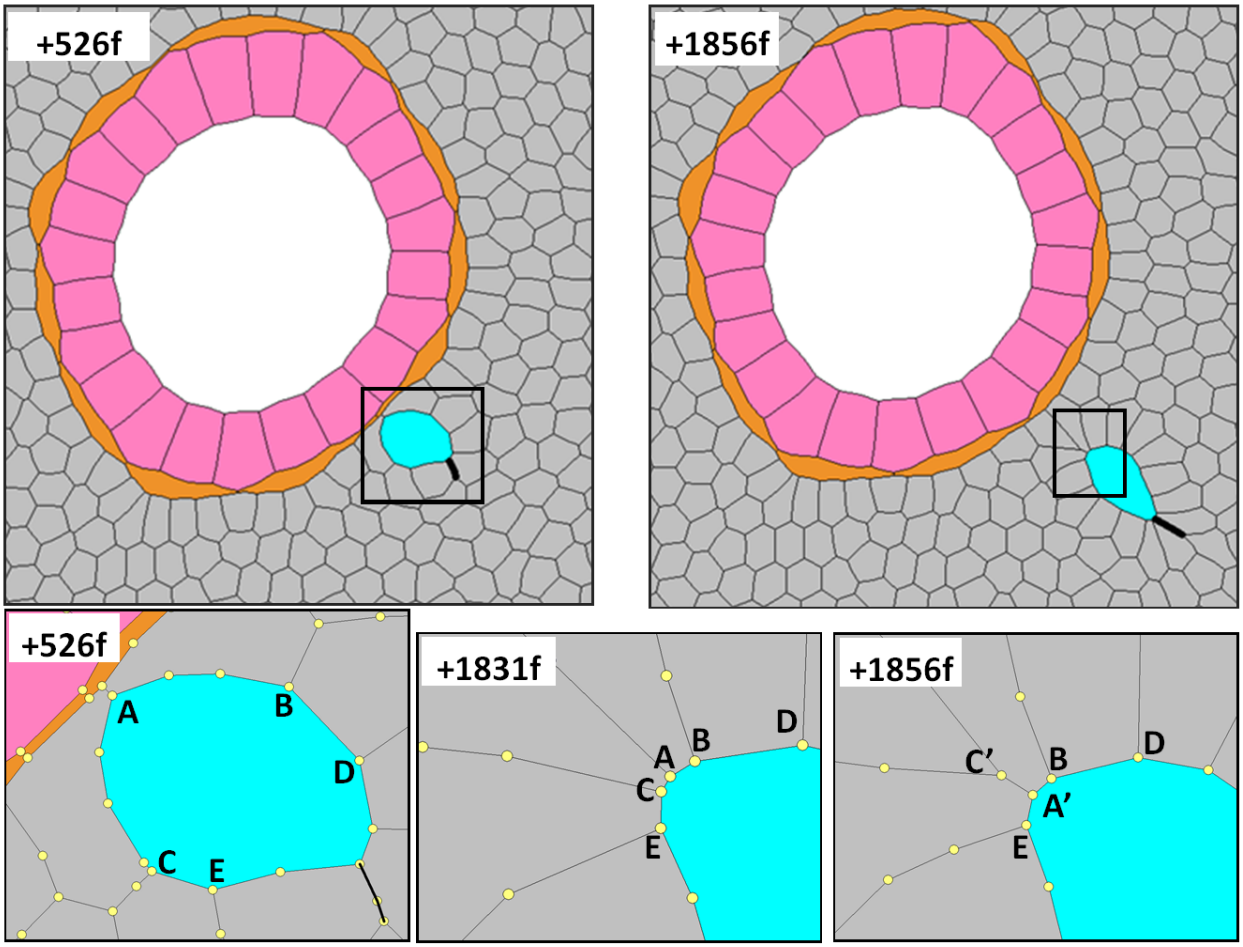

Figure 4.6: Escape Cell Migration in ECM with Protrusion Only ($\gamma^P = 1.5$)

4.3 Tension Gradient

The tension gradient studies showed that the Esc cell cannot detach from the duct as a result of tension gradients only. Once the Esc cell is in contact with the ECM, the Esc-ECM interface grows as the TG edges with higher tension at the rear pulls those TJs toward the rear end. However, after the simulation reaches the configuration shown in Figure 4.7, the Esc do not detach any further because:

$$\gamma^{TG-LE} < (\gamma^{LE-ME} + \gamma^{TG-ME})_{TG-LE\ axis}$$

When the model approaches the geometry shown in Figure 4.7; γ^{TG-LE} and γ^{TG-ME} are the tension gradient ITs bordering the LE and ME, respectively. In tension gradient, the IT increases gradually so the difference between γ^{TG-LE} and γ^{LE-ME} is low no matter the magnitude of the mean strength and

gradation. Therefore, when γ^{TG-ME} is added to γ^{LE-ME}, their force TG-LE axis is greater than γ^{TG-LE}. This equation is analogous to Condition 2 of MIT detachment, where the IT of the Esc-LE has to be higher than the sum of other Esc ITs for detachment. The tension gradient simulations were conducted with the mean strength ranging up to 4 with the degree of gradation of 1, and the Esc cell could not fully detach, but instead remained in geometries like that shown in Figure 4.7.

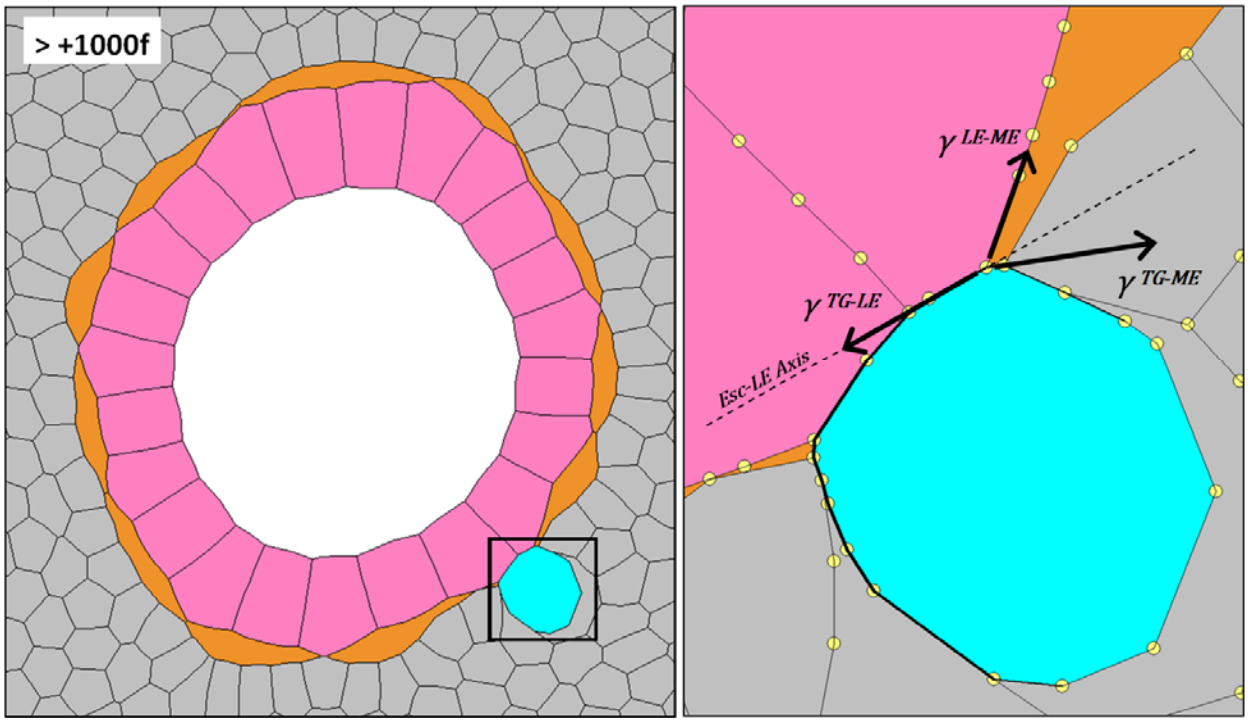

Figure 4.7: Typical Simulation Result of Esc Cell with Tension Gradient Only (Mean Strength = 2, Degree of Gradation = 1)

To test the effect of tension gradient on Esc cell migration in the ECM, it was applied to the Esc cell surrounded by the ECM after the MIT detachment (Figure 4.1, +50f). The Esc cell can migrate through ECM with only tension gradient after the detachment. This may seem counterintuitive as the Esc cell nodes displace toward the rear end of the Esc cell. Although the Esc edge nodes and TJs are moving toward the rear end, because the ECM elements consist of dashpot stiffness, they constitute as the anchorage for the Esc cell to move toward the outer edge of the ECM in the model. In Figure 4.8, the tension gradient mechanism pushes the Esc cell outward and pulls the ECM elements toward the back.

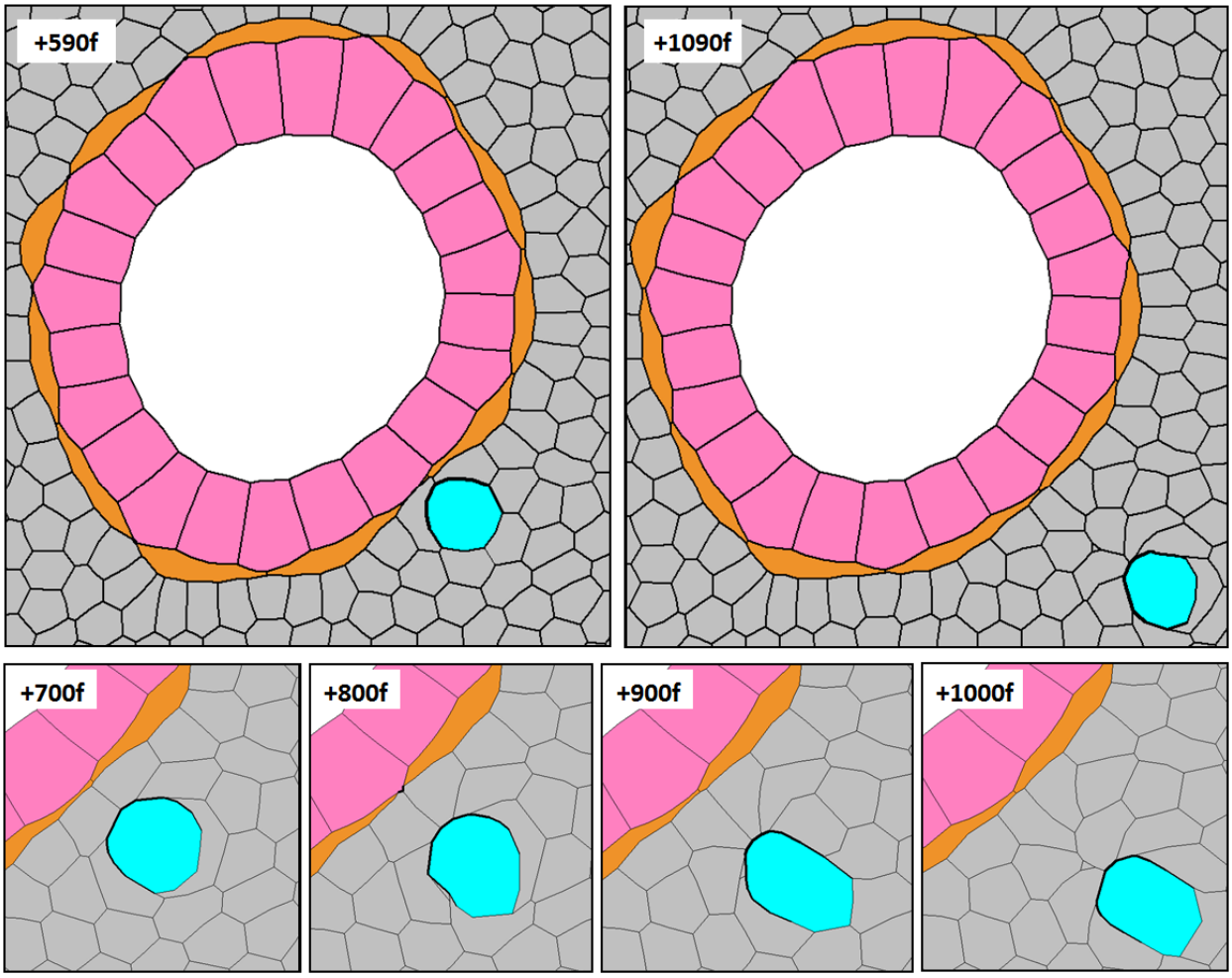

Figure 4.8: Escape Cell Migration in ECM with Tension Gradient Only (Mean Strength = 2, Degree of Gradation = 1)

4.4 Parametric Study of Combinations of Mechanisms

This section outlines the parametric studies of combinations of MIT, protrusion and tension gradient mechanisms. MIT and tension gradient are both mechanisms that are applied to the ITs of the Esc cell, hence they are assumed to occur mutually exclusive to each other. Thus the combined mechanisms included in this study are protrusions with either MIT or tension gradient.

Figure 4.9 presents the detachment time of the Esc cell when it is subjected to various γ^{Esc-ME} γ^{Esc-LE} and $\gamma^{Esc-Lumen}$ magnitudes and protrusion strengths. The x-axis is the same MIT multiplier from

Section 4.1, and y-axis is the IT of protrusion, γ^P. The plotted points are indicated with symbols that are coloured according to their respective detachment times. The plot shows that an Esc cell with an MIT multiplier of 0.6 can detach from the duct when a strong protrusion is present. Moreover, an Esc cell with a protrusion and MIT detaches from the duct in a shorter time than when it has only an MIT. The contribution of the protrusion is significant because it pulls the leading TJ with high IT, and its force is subsequently transmitted to the rest of the Esc cell nodes through the dashpots and stress fibres. Through the dashpots and stress fibres, all the rest of the Esc nodes displace more toward the protruding direction (Figure 4.10). As the protrusions makes the Esc cell-ECM interfaces orient more perpendicular to the duct perimeter, the increased angle between Esc-LE edge and Esc-LE axis reduces $(\gamma^{Esc-ME})_{Esc-LE}$, promoting a higher resultant in the direction of γ^{Esc-LE}.

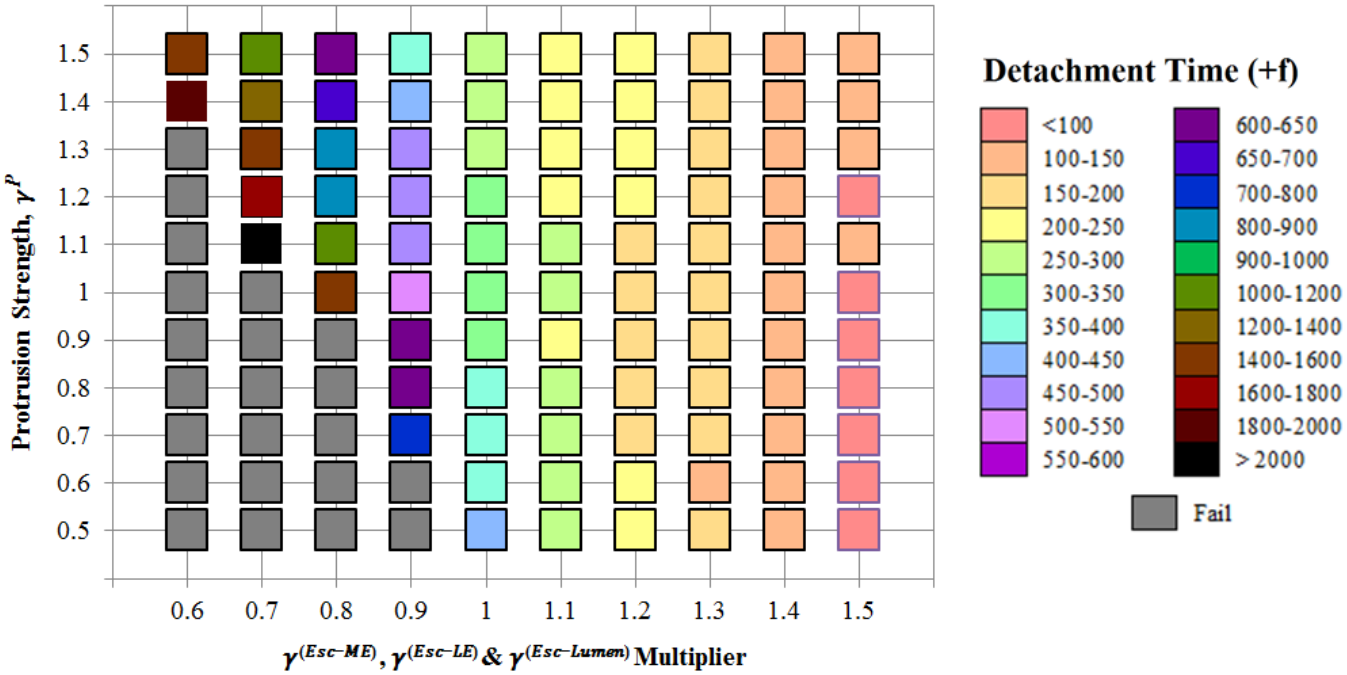

Figure 4.9: Detachment Time based on Protrusion Strength and MIT Multiplier

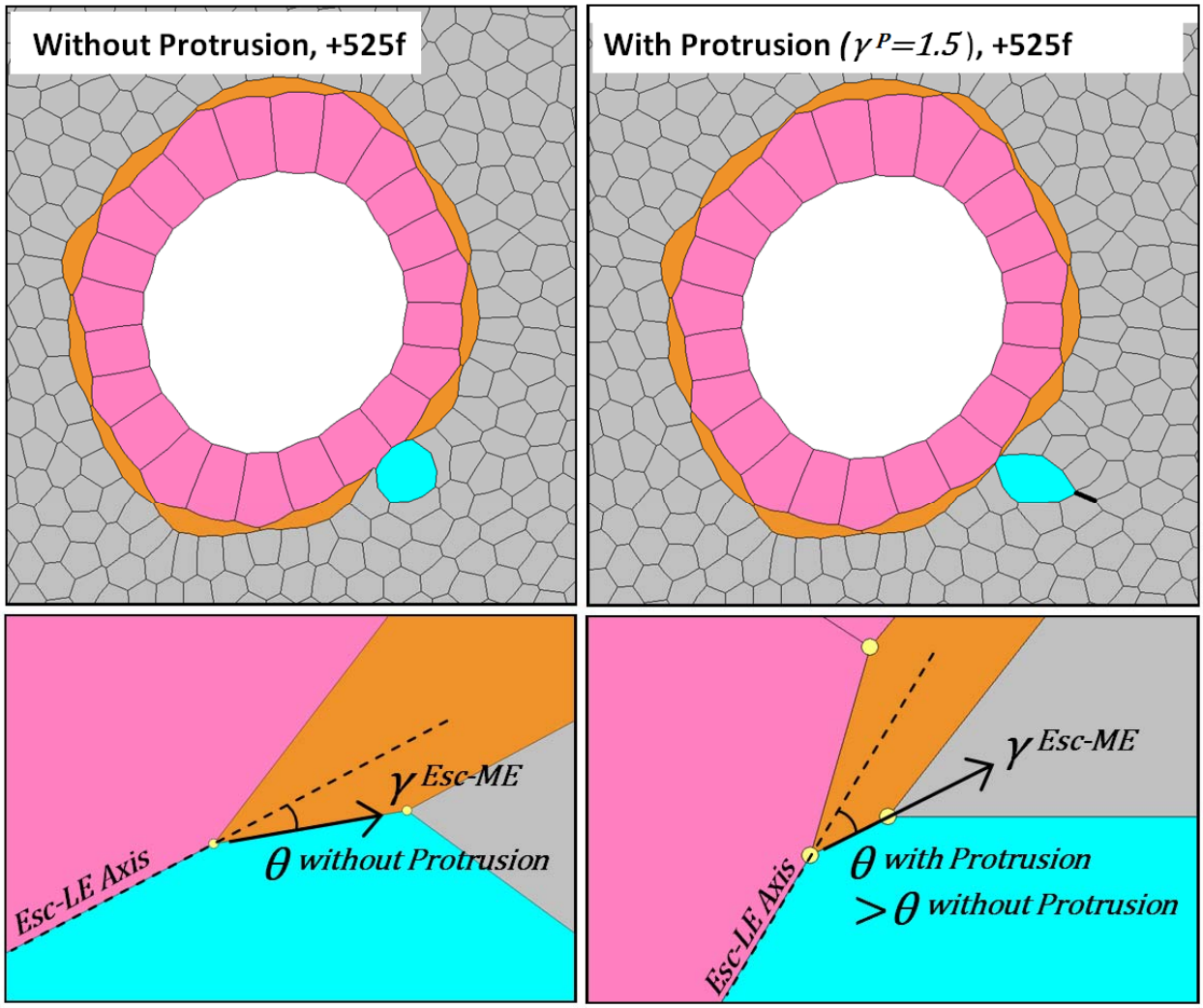

Figure 4.10: Escape Cell Geometry with and without Protrusion

Figure 4.11 shows the detachment time of the Esc cell based on the combination of varying strengths of protrusion and tension gradient gradation. The parametric study was conducted with the tension gradient mean strength of 1. The Esc cell can detach from the duct with the sufficiently strong combination of protrusion and tension gradient, and the detachment time decreases with increasing protrusion and tension gradient. The reason for the successful detachment when both protrusion and tension gradient are applied is the same as how the protrusion enabled the detachment of Esc with an MIT multiplier less than 1.

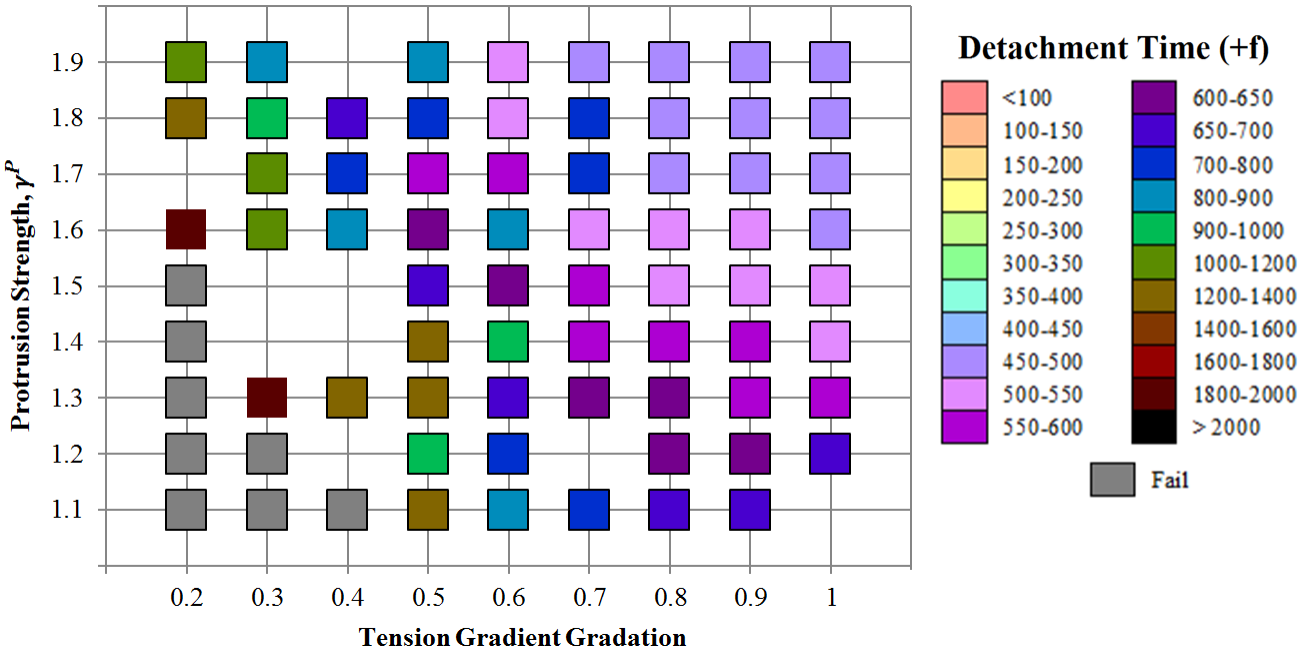

Figure 4.11: Detachment Time based on Protrusion Strength and Tension Gradient Gradation
(Note: Some data not shown for technical reasons)

Like the detachment process, combining protrusion and tension gradient mechanisms allows quicker and more effective migration of the Esc cell in the ECM. The forces of the protrusion and tension gradient exerted on the Esc cell nodes can be superpositioned, and therefore, the combined effect of two mechanisms is equivalent to the addition of their individual effects.

4.5 Discussion & Biological Implications

In the simulations of this study, the escape of the Esc cell can be considered to consist of two consecutive processes: detachment from the mammary duct and continuous migration through the ECM. This study has shown that MIT alone is sufficient for detachment, while protrusion alone or tension gradient alone are sufficient to produce migration through the ECM. Clearly, more than one mechanism are required to enable both detachment and migration of the Esc cell. Thus, one can draw the following conclusions regarding the roles of MIT, protrusion and tension gradient:

- An Esc cell can detach with either MIT alone, the combination of protrusion and MIT, or protrusion and tension gradient.

- An Esc cell can migrate through ECM with protrusion alone, tension gradient alone, the combination of protrusion and MIT, or protrusion and tension gradient.

The reason the protrusion alone and tension gradient alone failed in detachment is because they could not satisfy the Condition 2 from Section 4.1, which was developed for MIT. Condition 1 and 2 from Section 4.1 do not only apply to MIT but are ubiquitous conditions of ITs required to be fulfilled for the complete detachment of the Esc cell from the duct. There is no single mechanism that alone can cause the Esc cell to both detach from the duct and migrate through the ECM. The parametric studies indicate that when in combination, the strength of each mechanism can be weaker for the Esc cell to escape. Also, the differences of ITs of the detaching Esc cell dictate whether the mammary duct remains disfigured or reorganizes itself.

These analyses are based on the ITs assumed in the homeostatic case. Simulations based on other values could produce modified results, but most of the findings would be expected to stand, given the modest range within which the IT values must fall to satisfy the IT conditions from Section 3.1.2.

Consider the mouse mammary duct experiment discussed in Section 2.2.3, where LE cell behaviours were observed after removal of E-cadherin and introduction of Twist1. In the case of E-cadherin deletion, the duct loses its circularity as the outer LE cells become more exposed to the Matrigel. This phenomenon resembles the model result shown in Figure 4.7 from Section 4.3, where the ITs bordering the Esc and other cells significantly increase but not strong enough for the detachment. As the DITH equations state, increase in cell-cell adhesion decreases IT, suggesting that the semi-LE detachment of the LE cells is due to the significant decrease of cell-to-cell adhesion. Neumann et al. (In preparation) found that Twist1 alters the cell-to-ECM interaction significantly. In terms of the DITH, it is also possible to cause detachment of an Esc cell from the duct and migration through the ECM of a LE cell using protrusion and weakening Esc cell-ECM IT. The DITH-based FE simulation have replicated the

mechanisms of a metastatic cell, and through that, fully supports the real-world biological experiments. These harmonies with biological experiments suggest that other findings from this study, such as how a LE cell cannot detach from the duct but can migrate through ECM with protrusion or tension gradient only, though as yet untestable, could also have biological relevance.

Chapter 5 : Conclusions & Recommendations

This study has been able to address the main questions posed in the Introduction chapter, specifically:

1. *What is the mechanical cause of LE cell escape in terms of the DITH?*

   A single metastatic LE cell must accomplish of two consecutive actions – detachment from the mammary duct and continuous migration in ECM – in order to successfully escape from a mammary duct. Through the DITH-based FE simulations, it was found that the Esc cell requires strong rear end ITs to detach from its adjacent LE and ME cells and lumen to gain access to the ECM. Moreover, the Esc cell requires special mechanisms that continuously generate high tension edges such as protrusion or tension gradient, to migrate through the ECM.

2a. *What metastatic traits are required for a LE cell to escape from the mammary duct?*

   A metastatic cell needs either of the followings to detach from the mammary duct: a combination of protrusion and tension gradient, or any other mechanisms that significantly increase contractions of or reduce adherences between the Esc cell and its neighbouring cells and ECM. The Esc cell can migrate through ECM with strong protrusion or tension gradient singly or in combination.

2b. *Can the mechanisms exhibited by the embryonic LE cells from mammary duct development also drive cancer metastasis?*

   Yes, a metastatic cell that reactivates the protrusion and tension gradient mechanisms used to construct the duct during early morphogenesis can escape from the mammary duct. The difference is that the Esc cell requires both mechanisms active, whereas the embryonic LE cells need only one of the two mechanisms to intercalate.

Furthermore, in mammary gland development, protrusion and tension gradients in an intercalating LE cell cease as soon as it touches a ME cell, but in the metastatic escape, at least one of these mechanisms must stay active.

Many studies of metastasis focus on cell-to-cell and cell-to-ECM interactions and individual traits of metastatic cells; the DITH-based FE software showed that the mechanics of multiple cells must be considered at the same time. The simulations demonstrate that the protrusion and tension gradient mechanisms involved in embryonic mammary duct development have the capacity to drive metastatic cell escape if reactivated. In future, as more is known about the mechanical properties of the cells and ECM, these aspects of the simulations can be further strengthened.

It is hoped that these findings will lead to further studies of the mechanics of metastasis and that they will eventually to improved clinical strategies to reduce the incidence of metastasis.

References

Adriance, M. C., Inman, J. L., Petersen, O. W., & Bissell, M. J. (2005). Myoepithelial cells: good fences make good neighbors. *Breast Cancer Research : BCR*, *7*(5), 190–197. https://doi.org/10.1186/bcr1286

American Caner Society. (2016). Types of Breast Cancers. Retrieved April 18, 2017, from http://www.cancer.org/cancer/breastcancer/detailedguide/breast-cancer-breast-cancer-types

Armstrong, P. B. (1989). Cell Sorting Out: The Self-Assembly of Tissues In Vitro. *Critical Reviews in Biochemistry and Molecular Biology*, *24*(2), 119–149. https://doi.org/10.3109/10409238909086396

Bane, A. (2013). Ductal Carcinoma In Situ : What the Pathologist Needs to Know and Why, *2013*.

Blanchoin, L., Boujemaa-Paterski, R., Sykes, C., & Plastino, J. (2014). Actin Dynamics, Architecture, and Mechanics in Cell Motility. *Genetics*, *160*(3), 923–934. https://doi.org/10.1152/physrev.00018.2013

Borghi, N., Shcherbakova, O. G., Weis, W. I., Pruitt, B. L., James, W., Dunn, A. R., … Dunn, A. R. (2012). Correction for Borghi et al., E-cadherin is under constitutive actomyosin-generated tension that is increased at cell-cell contacts upon externally applied stretch. *Proceedings of the National Academy of Sciences*, *109*(46), 19034–19034. https://doi.org/10.1073/pnas.1217417109

Brodland, G. W. (2006). Do lamellipodia have the mechanical capacity to drive convergent extension? *International Journal of Developmental Biology*, *50*(2–3), 151–155. https://doi.org/10.1387/ijdb.052040gb

Brodland, G. W., & Chen, H. H. (2000a). The mechanics of cell sorting and envelopment. *Journal of Biomechanics*, *33*(7), 845–851. https://doi.org/10.1016/S0021-9290(00)00011-7

Brodland, G. W., & Chen, H. H. (2000b). The mechanics of heterotypic cell aggregates: insights from computer simulations. *Journal of Biomechanical Engineering*, *122*(4), 402–7. https://doi.org/10.1115/1.1288205

Brodland, G. W., & Veldhuis, J. H. (2006). Lamellipodium-driven tissue reshaping: a parametric study. *Computer Methods in Biomechanics and Biomedical Engineering*, *9*(1), 17–23. https://doi.org/10.1080/10255840600554703

Brodland, G. W., Veldhuis, J. H., Kim, S., Perrone, M., Mashburn, D., & Hutson, M. S. (2014). CellFIT: A cellular force-inference toolkit using curvilinear cell boundaries. *PLoS ONE*, *9*(6). https://doi.org/10.1371/journal.pone.0099116

Brodland, G. W., Viens, D., & Veldhuis, J. H. (2007). A new cell-based FE model for the mechanics of embryonic epithelia. *Computer Methods in Biomechanics and Biomedical Engineering*, *10*(2), 121–128. https://doi.org/10.1080/10255840601124704

Brodland, W. (2002). The Differential Interfacial Tension Hypothesis (DITH): a comprehensive theory for the self-rearrangement of embryonic cells and tissues. *Journal of Biomechanical Engineering*, *124*(2), 188–197. https://doi.org/10.1115/1.1449491

Brodland, W. (2004). Computational modeling of cell sorting, tissue engulfment, and related phenomena: A review. *Applied Mechanics Reviews*, *57*(1), 47. https://doi.org/10.1115/1.1583758

Brodland, W. (2015). How computational models can help unlock biological systems. *Seminars in Cell and Developmental Biology*, *47–48*, 62–73. https://doi.org/10.1016/j.semcdb.2015.07.001

Brodland, W., Chen, X., Lee, P., Marsden, M., (2010). From genes to neural tube defects (NTDs): Insights from multiscale computational modeling. *HFSP Journal*, 4, 142-152. http://dx.doi.org/10.2976/1.3338713

Brodland, W., & Veldhuis, J. H. (2012). The Mechanics of Metastasis: Insights from a Computational Model. *PLoS ONE*, *7*(9). https://doi.org/10.1371/journal.pone.0044281

Campàs, O., Mammoto, T., Hasso, S., Sperling, R. A., O'Connell, D., Bischof, A. G., … Ingber, D. E. (2014). Quantifying cell-generated mechanical forces within living embryonic tissues. *Nature Methods*, *11*(2), 183–9. https://doi.org/10.1038/nmeth.2761

Cancer Research UK. (2014). *World cancer factsheet: World cancer burden (2012)* (Vol. 2012).

Chambers, A. F., Groom, A., & MacDonald, I. C. (2003). DISSEMINATION AND GROWTH OF CANCER CELLS IN METASTATIC SITES. *Clinical Cancer Research*, *9*(15), 5607–5615. https://doi.org/10.1038/nrc865

Chen, H. H. (2000). Cell-Level Finite Element Studies of Viscous Cells in Planar Aggregates. *Journal of Biomechanical Engineering*, *122*(4), 394. https://doi.org/10.1115/1.1286563

Chen, X., & Brodland, W. (2009). Mechanical determinants of epithelium thickness in early-stage embryos. *Journal of the Mechanical Behavior of Biomedical Materials*, *2*(5), 494–501. https://doi.org/10.1016/j.jmbbm.2008.12.004

Chidgey, M., & Dawson, C. (2007). Desmosomes: a role in cancer? *British Journal of Cancer*, *96*(12), 1783–1787. https://doi.org/Doi 10.1038/Sj.Bjc.6603808

Dachs, G. U., Dougherty, G. J., Stratford, I. J., & Chaplin, D. J. (1997). Targeting gene therapy to cancer: A review. *Oncology Research*, *9*(6–7), 313–325. Retrieved from http://www.ncbi.nlm.nih.gov/pubmed/9406237

El-Aneed, A. (2004). An overview of current delivery systems in cancer gene therapy. *Journal of Controlled Release*. https://doi.org/10.1016/j.jconrel.2003.09.013

Genetics Home Reference. (2017). TWIST 1 gene. Retrieved on June 8, 2017 from https://ghr.nlm.nih.gov/gene/TWIST1

Guo, J., Sachs, F., & Meng, F. (2014). Fluorescence-based force/tension sensors: a novel tool to visualize mechanical forces in structural proteins in live cells. *Antioxidants & Redox Signaling*, *20*(6), 986–99. https://doi.org/10.1089/ars.2013.5708

Hiiragi, T., Veldhuis, J. H., Ehsandar, A., Cox, S., & Brodland, W. (2017). Inferring cellular forces from image stacks. https://doi.org/10.1098/rstb.2016.0261

Huebner, R. J., & Ewald, A. J. (2014). Cellular foundations of mammary tubulogenesis. *Seminars in Cell and Developmental Biology*, *31*, 124–131. https://doi.org/10.1016/j.semcdb.2014.04.019

Hutson, M. S., Veldhuis, J., Ma, X., Lynch, H. E., Cranston, P. G., & Brodland, W. (2009). Combining laser microsurgery and finite element modeling to assess cell-level epithelial mechanics. *Biophysical Journal*, *97*(12), 3075–3085. https://doi.org/10.1016/j.bpj.2009.09.034

J, N. Dxm. (2007). Genetic determinants of cancer metastasis. *Nature Reviews. Genetics*, *8*(5), 341–352. https://doi.org/10.1038/nrg2101

Kasza, K. E., Vader, D., Köster, S., Wang, N., & Weitz, D. A. (2011). Magnetic twisting cytometry. *Cold Spring Harbor Protocols*, *6*(4). https://doi.org/10.1101/pdb.prot5599

Krens, S. F. G., Veldhuis, J. H., Barone, V., Capek, D., Maitre, J.-L., Brodland, G. W., & Heisenberg, C. P. (2017). Interstitial fluid osmolarity modulates the action of differential tissue surface tension in progenitor cell segregation during gastrulation. *The Company of Biologists Ltd*, *Developmen*((In Submission)). https://doi.org/10.1098/rsbl.2009.0501

Legant, W. R., Miller, J. S., Blakely, B. L., Cohen, D. M., Genin, G. M., & Chen, C. S. (2010). Measurement of mechanical tractions exerted by cells in three-dimensional matrices. *Nature Methods*, *7*(12),

969–71. https://doi.org/10.1038/nmeth.1531

Lewis, R., Nithiarasu, P., & Seetharamu, K. (2004). *Fundamentals of the finite element method for heat and fluid flow*. *Wiley*. https://doi.org/10.1002/0470014164

Macias, H., & Hinck, L. (2012). Mammary Gland Development. *Wiley Interdisciplinary Reviews: Developmental Biology*, *1*(4), 533–557. https://doi.org/10.1002/wdev.35.Mammary

Maître, J.-L., Berthoumieux, H., Krens, S. F. G., Salbreux, G., Jülicher, F., Paluch, E., … Heisenberg, C.-P. C.-P. (2012). Adhesion Functions in Cell Sorting by Mechanically Coupling the Cortices of Adhering Cells. *Science (New York, N.Y.)*, *338*(6104), 253–6. https://doi.org/10.1126/science.1225399

Maître, J.-L., Niwayama, R., Turlier, H., Nédélec, F., & Hiiragi, T. (2015). Pulsatile cell-autonomous contractility drives compaction in the mouse embryo. *Nature Cell Biology*, *17*(7), 849–855. https://doi.org/10.1038/ncb3185

Mazumdar, M. D. (n.d.). Anatomy of the Female Breast. Retrieved April 18, 2017, from http://www.breastcancertreatment.in/breast_anatomy.htm

Mehlen, P., & Puisieux, A. (2006). Metastasis: a question of life or death. *Nature Reviews. Cancer*, *6*(6), 449–58. https://doi.org/10.1038/nrc1886

Monk, M., & Holding, C. (2001). Human embryonic genes re-expressed in cancer cells, (August), 9232.

Morimatsu, M., Mekhdjian, A. H., Adhikari, A. S., & Dunn, A. R. (2013). Molecular tension sensors report forces generated by single integrin molecules in living cells. *Nano Letters*, *13*(9), 3985–3989. https://doi.org/10.1021/nl4005145

National Breast Cancer Foundation Inc. (2016). Metastatic Breast Cancer. Retrieved from http://www.nationalbreastcancer.org/metastatic-breast-cancer

Neumann, N. M., Perrone, M. C., Veldhuis, J. H., Zhan, H., Devreotes, P. N., Brodland, G. W., & Ewald, A.

J. (n.d.). Coordination of receptor tyrosine kinase signaling and interfacial tension dynamics drive radial intercalation and tube elongation. *Development Cell*, (In Submission).

Perrone, M. C., Veldhuis, J. H., & Brodland, G. W. (2016). Non-straight cell edges are important to invasion and engulfment as demonstrated by cell mechanics model. *Biomechanics and Modeling in Mechanobiology*, *15*(2), 405–418. https://doi.org/10.1007/s10237-015-0697-6

Potts, D. M., & Zdravkovic, L. (2001). *Finite Element Analysis in Geotechnical Engineering Application*. London: Thomas Telford.

RnCeus. (n.d.). No Title. Retrieved from http://www.rnceus.com/dcis/sub.html

Roses, R. E., Arun, B. K., Lari, S. A., Mittendorf, E. A., Lucci, A., Hunt, K. K., & Kuerer, H. M. (2011). Ductal carcinoma-in-situ of the breast with subsequent distant metastasis and death. *Annals of Surgical Oncology*, *18*(10), 2873–8. https://doi.org/10.1245/s10434-011-1707-2

Shamir, E. R., Pappalardo, E., Jorgens, D. M., Coutinho, K., Tsai, W. T., Aziz, K., … Ewald, A. J. (2014). Twist1-induced dissemination preserves epithelial identity and requires E-cadherin. *Journal of Cell Biology*, *204*(5), 839–856. https://doi.org/10.1083/jcb.201306088

Standring, S. (2008). *Gray's Anatomy: The Anatomical Basis of Clinical Practice*. *Development* (Vol. 2). https://doi.org/10.1097/ACM.0b013e31819391e2

Stéhelin, D. (1995). Oncogenes and cancer. *Science (New York, N.Y.)*, *267*(5203), 1408–1409. https://doi.org/10.1126/science.7878455

Steinberg, M. S. (1975). Adhesion-guided multicellular assembly: a commentary upon the postulates, real and imagined, of the differential adhesion hypothesis, with special attention to computer simulations of cell sorting. *Journal of Theoretical Biology*, *55*(2), 431–443. https://doi.org/10.1016/S0022-5193(75)80091-9

Steinberg, M. S. (2007). Differential adhesion in morphogenesis: a modern view. *Current Opinion in Genetics and Development*, *17*(4), 281–286. https://doi.org/10.1016/j.gde.2007.05.002

Sternlicht, M. D. (2006). Key stages in mammary gland development: the cues that regulate ductal branching morphogenesis. *Breast Cancer Research : BCR*, *8*(1), 201. https://doi.org/10.1186/bcr1368

Sugimura, K., Graner, F., & Lenne, P.-F. (2015). Measuring forces and stresses in situ in living tissues. *bioRxiv*, (Table 1), 16394. https://doi.org/10.1101/016394

Tambe, D. T., Croutelle, U., Trepat, X., Park, C. Y., Kim, J. H., Millet, E., … Fredberg, J. J. (2013). Monolayer Stress Microscopy: Limitations, Artifacts, and Accuracy of Recovered Intercellular Stresses. *PLoS ONE*, *8*(2). https://doi.org/10.1371/journal.pone.0055172

Thomas, G., Burnham, N. a, Camesano, T. A., & Wen, Q. (2013). Measuring the mechanical properties of living cells using atomic force microscopy. *Journal of Visualized Experiments : JoVE*, (76), 1–8. https://doi.org/10.3791/50497

Vedula, S. R. K., Hirata, H., Nai, M. H., Brugués, A., Toyama, Y., Trepat, X., … Ladoux, B. (2014). Forces driving epithelial wound healing. *Nature Physics*, *10*(1), 683–690. https://doi.org/10.1038/nmat3814

Ventura, A., & Merajver, S. (2008). Genetic determinants of aggressive breast cancer. *Annual Review of Medicine*, *59*, 199–212. https://doi.org/10.1146/annurev.med.59.060106.184830 [doi]

Viens, D., & Brodland, W. (2007). A Three-dimensional Finite Element Model for the Mechanics of Cell-Cell Interactions. *Journal of Biomechanical Engineering*, *129*(5), 651. https://doi.org/10.1115/1.2768375

Wasif, N., Maggard, M. A., Ko, C. Y., & Giuliano, A. E. (2010). Invasive lobular vs. ductal breast cancer: a

stage-matched comparison of outcomes. *Annals of Surgical Oncology*, *17*(7), 1862–9. https://doi.org/10.1245/s10434-010-0953-z

Zienkiewicz, O. C., Taylor, R. L., & Fox, D. (2014). The Finite Element Method for Solid and Structural Mechanics. *The Finite Element Method for Solid and Structural Mechanics*, *2*, 215–233. https://doi.org/10.1016/B978-1-85617-634-7.00007-7

Zienkiewicz, O. C., Taylor, R. L., & Nithiarasu, P. (2014). The Finite Element Method for Fluid Dynamics. *The Finite Element Method for Fluid Dynamics*, 1–29. https://doi.org/10.1016/B978-1-85617-635-4.00001-7

Zijl, F. V., Krupitza, G., & Mikulits, W. (2011). Initial Steps of Metastasis: Cell Invation and Endothelial Transmigration. *Mutation Research*, 728.

Glossary

Cytoskeleton

The main structural and force exerting components of a cell, including actin filaments and keratin networks.

Dashpot Approach

An approach for representing the effective viscosity of cytoplasm and other contents of the cell.

Differential Interfacial Tension Hypothesis (DITH)

Theory for rearrangement of cells through the effects of interfacial tensions.

DITH-based Finite Element (FE) Method

A finite element implementation developed by the Brodland lab to simulate cell deformation and rearrangement.

E-cadherin

One of several molecules that provides adhesion between cells.

Edge Node

A node that joins the same interface edges.

Edge Node Addition (ENA)

A feature of DITH-based FE software that adds an extra edge node between two adjacent nodes when the distance between them exceeds than a specified maximum node-to-node distance.

Edge Node Removal (ENR)

A feature of DITH-based FE software that removes one of two adjacent nodes when the distance between them becomes lower than a specified minimum node-to-node distance.

Epithelial Cell

A cell that forms layered tissue structure to enclose and protect organs.

Extracellular Matrix (ECM)

Tissue made of protein fibres such as collagen and protein secreting cells such as fibroblasts.

Homeostasis

The status of a collection of cells maintaining a regulated constant activity. Homeostatic cells in a tissue do not exhibit any substantial morphological rearrangement, with the exception of mitosis and apoptosis.

Invasive Ductal Carcinoma (IDC)

A type of breast cancer in which certain LE cells leave the duct structure.

Interface

The contact area formed between two elements, such as cells or matrix.

Interfacial Tension (IT)

The tensile force that arises in a cell-to-cell or cell-to-matrix interface. It is denoted by γ^{XY}, when the interface is formed by contacting X and Y elements.

Luminal Epithelial (LE) Cell

An epithelial cell in a mammary (breast) duct and lobe. LE cells in mammary lobes secrete breast milk during a lactation period.

Mammary Duct

A duct in mammary gland that delivers the milk to the nipple

Mammary Gland

An organ that produces and secretes breast milk; consists of mammary lobes, ducts and a nipple

Metastasis

The process of cancer cells spreading from their original tumour and invading other organs

Modified Interfacial Tension (MIT)

Changes to ITs in a DITH-based FE model.

Morphology

The description of cell and tissue structure.

Myoepithelial (ME) Cell

An epithelial cell in a mammary duct that enclose LE cells. ME cells in the mammary ducts contract and expand during a lactation period.

Neighbour Change

A feature of the FE software which removes two approaching triple junctions (TJ) when the distance between them becomes lower than a set distance, and creates a new pair of TJs to establish the new cell contacts.

Protrusion

An extension of cell membrane that protrudes between other cells or ECM. The end of the protrusion may attach to another cell or to ECM, and it can pull the protrusive cell as it contracts.

Stress Fibre

A network of actin filaments that retract the rear portion of a protruding cell.

Tension Gradient

A trait of migrating cells in which actin filaments are more strongly contracting in its posterior membrane than in its leading portion.

Triple junction (TJ)

A node that joins three edges of different interfaces.

Twist1

A transcription factor that turns the epithelial structure of LE cells into mesenchymal (fluid) structure; Twist1 induces LE cells to disseminate from the mammary duct.